Fractal-Based Point Processes

2005

Steven Bradley Lowen
Harvard Medical School
McLean Hospital

Malvin Carl Teich
Boston University
Columbia University

WILEY

11

Operations

The famous Swiss mathematician **Jakob Bernoulli (1654–1705)** conceived of a sequence of statistical trials, each of which yields one of two mutually exclusive outcomes ("heads" or "tails"), with probabilities that are fixed across trials.

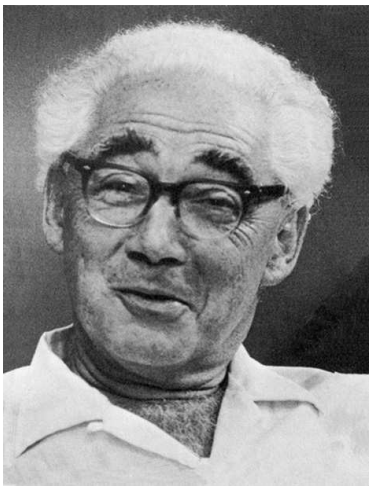

The celebrated probabilist **William Feller (1906–1970)**, who studied at Zagreb and Göttingen, made significant advances in many areas of probability, including Brownian motion, diffusion theory, and dead-time-modified counting processes.

A number of transformations exist by means of which one or more point processes $\{dN_1(t), \ldots, dN_n(t)\}$ are converted into a new point process $dN_R(t)$. We focus on six such operations in the context of fractal and fractal-rate point processes:

- **Dilation**, which involves contracting or expanding the time axis of a counting process.
- **Deletion**, which eliminates selected events of a point process according to a specified rule, examples of which include:
  1. Retaining every ℓ th event with all others eliminated (**decimation**);
  2. Subjecting each event to an independent Bernoulli trial in which it is deleted with a fixed probability (**random deletion** or **thinning**);
  3. Eliminating events if they follow other events more closely than a specified time interval (**dead-time deletion** or **refractoriness deletion**).
- **Displacement**, where we modify the occurrence time of each event of a point process in a specified manner, for example by jitter.
- **Interval transformation**, where the ordering of the intervals remains unchanged but we transform the interval density to a different form, for example an exponential density.
- **Shuffling**, where we randomize the interevent-interval ordering in a particular way, while the interval probability density is constrained:

1. We randomly reorder the intervals and preserve the original interval density (**full shuffling**);

2. We randomly reorder the intervals within blocks of a realization and retain the original interval density (**block shuffling**);

3. We select intervals with replacement, thereby generating a renewal process (**bootstrap method**).

- **Superposition**, which forms a new point process from the sum of a collection of point processes.

Transformations such as these play important roles in the identification of point processes. In some cases, they are inherent in the measured events. This can occur because: (1) they are intrinsic to the underlying process; (2) they are unavoidably imposed by the detection/measurement system recording the events. Commonly encountered operations in the physical and biological sciences include Bernoulli random deletion, dead-time deletion, displacement, and superposition.[1]

In other cases, experimenters deliberately use such transformations to create surrogate data sets that are useful for elucidating the underlying nature of an observed point process[2] (Schiff & Chang, 1992; Theiler, Eubank, Longtin, Galdrikian & Farmer, 1992; Ott et al., 1994). The shuffling and exponentialization operations, for example, prove valuable for determining whether the fractal behavior observed in a sequence of action potentials stems from the form of the interevent-interval density, the ordering of the intervals, or both.[3] Examples that illustrate these operations appear throughout this chapter.

Operations such as decimation and dead-time deletion are also sometimes used to deliberately reduce the variability of a point process [see, for example, Saleh & Teich (1985b) and Teich & Cantor (1978), respectively].

We devote this chapter to determining the effect of each of these transformations on the relevant point-process statistics, and illustrating how these operations affect the nature of fractal and fractal-rate point processes.

[1] Examples in which these four transformations are intrinsic to the underlying process appear in Teich & Khanna (1985); Teich, Matin & Cantor (1978); Teich et al. (2001); and Palm (1943), respectively. Examples in which they are imposed in the course of measurement appear in Teich & Saleh (1982); Teich & Vannucci (1978); Teich, Khanna & Guiney (1993); and Abeles, de Ribaupierre & de Ribaupierre (1983), respectively.

[2] The creation of surrogate data resembles the creation of "knockout mice," a biological procedure developed in the mid-1980s to study gene function (see Evans, Smithies & Capecchi, 2001). Knockout animals are created by replacing a specific natural gene with an inactive or mutated allele. The behavior or performance of the "surrogate mouse" provides information about the role played by the gene.

[3] Other operations also create useful surrogates. Phase randomization in the Fourier domain, for example, preserves the spectral magnitude and therefore the second-order properties of a point process. Since this procedure removes other temporal structure, it yields information about the presence or absence of deterministic chaos in a system [see, for example, Turcott & Teich (1996) and Teich et al. (2001)].

11.1 TIME DILATION

Time dilation is, perhaps, the simplest of operations that can be carried out on a point process (Papangelou, 1972). The time axis t of a counting process is expanded or contracted by a factor c that is, respectively, larger or smaller than unity:

$$N_R(t) = N_1(t/c). \tag{11.1}$$

Forming the point process as the derivative of the counting process introduces an additional factor[4] of $1/c$,

$$dN_R(t) = c^{-1}\, dN_1(t/c). \tag{11.2}$$

This factor carries through to the statistics of the point process in a straightforward manner. Four cases exist, depending on whether the measure or its arguments (if any) has dimensions of real time (sec) or frequency (Hz). The simplest case obtains when the statistic neither has units, nor takes arguments with units, as is true for the interval-based skewness, kurtosis, rescaled range, and generalized dimensions. For these statistics, dilation causes no change.

We next consider the case where the measure itself has no units but takes arguments that do. These follow relations similar to those for the point process as a whole:

$$\begin{array}{lrcl}
\text{interval distribution} & P_{\tau R}(t) & = & P_{\tau 1}(t/c) \\
\text{normalized count variance} & F_R(T) & = & F_1(T/c) \\
\text{normalized wavelet count variance} & A_R(T) & = & A_1(T/c) \\
\text{count autocorrelation} & R_{ZR}(k,T) & = & R_{Z1}(k,T/c).
\end{array} \tag{11.3}$$

Some interval statistics do have units, but do not take arguments with units, which leads to multiplicative factors for the measures themselves:

$$\begin{array}{lrcl}
\text{interval moments} & \mathrm{E}[\tau_R^n] & = & c^n\, \mathrm{E}[\tau_1^n] \\
\text{interval variance} & \mathrm{Var}[\tau_R] & = & c^2\, \mathrm{Var}[\tau_1] \\
\text{interval autocorrelation} & R_{\tau R}(k) & = & c^2\, R_{\tau 1}(k) \\
\text{interval spectrum} & S_{\tau R}(\mathsf{f}) & = & c^2\, S_{\tau 1}(\mathsf{f}),
\end{array} \tag{11.4}$$

and similarly for the interval wavelet variance.

Finally, for statistics that have units and also take arguments with units, multiplicative factors appear in the measures themselves as well as in their arguments:

$$\begin{array}{lrcl}
\text{interval probability density} & p_{\tau R}(t) & = & c^{-1}\, p_{\tau 1}(t/c) \\
\text{coincidence rate} & G_R(t) & = & c^{-2}\, G_1(t/c) \\
\text{point-process spectrum} & S_{NR}(f) & = & c^{-1}\, S_{N1}(cf) \\
\text{general-wavelet variance} & \mathrm{Var}[C_{\psi,NR}(a,b)] & = & c^{-1}\, \mathrm{Var}[C_{\psi,N1}(a/c, b/c)].
\end{array} \tag{11.5}$$

[4] However, the delta functions that comprise $dN_R(t)$ do not change since $a\delta(at) = \delta(t)$ for all positive, finite a, as discussed in Sec. 4.4.

The foregoing establishes that dilation simply alters the relevant time scales. It does not convert a fractal point process into a fractal-rate point process, nor the opposite. All of the fractal-based point processes we consider therefore retain their form under time dilation and maintain their scaling exponents, although intrinsic times (and frequencies) such as the mean interval and fractal onset time change by the factor c.

11.2 EVENT DELETION

Event deletion forms another class of operations on point processes. We consider three subclasses of deletion that differ in how events are selected for elimination: (1) **Decimation**, in which every ℓ th event survives while all others do not; (2) **Random deletion**, where each event survives with a probability r that is independent of the survivals of other events and of the point process itself; and (3) **Dead-time deletion**, in which the probability of survival of an event $r(t)$ resets to zero following each surviving event, and thence increases monotonically to unity. Figure 11.1 schematically illustrates how these three types of event deletion operate on a representative point process.

11.2.1 General results

How does the deletion of events affect a fractal or fractal-rate point process? Assuming that the deletion probability does not itself exhibit significant long-term fluctuations,[5] the deleted process, although altered, remains a member of the fractal family of point processes with the same fractal exponent.

To understand how this comes about, consider a fractal or fractal-rate point process with mean interevent time $\mathrm{E}[\tau_1]$, fractal exponent α_1, and fractal onset frequency f_{S1}. Over a range of frequencies, the spectrum follows the form of the mid-frequency term in Eq. (5.44a):

$$S_{N1}(f) \approx \mathrm{E}[\mu_1]\,(f/f_{S1})^{-\alpha_1}. \tag{11.6}$$

Suppose now that we retain some proportion r of the events in $dN_1(t)$ to form $dN_R(t)$, where the selection probability of these points is devoid of low-frequency components. Decimation and random deletion, discussed in Secs. 11.2.2 and 11.2.3, respectively, do not selectively alter the low-frequency components of the process so that the following considerations apply to these deletion processes. On the other hand, dead-time deletion, discussed in Sec. 11.2.4, violates this condition so that

[5] We mention this caveat since such behavior can affect the fractal characteristics of a point process. Suppose, for example, that $dN_1(t)$ belongs to the homogeneous Poisson-process family and that the deletion process selects events from $dN_1(t)$ with a probability $r(t)$ described by a fractal Gaussian process. The resultant deleted process $dN_R(t)$ then belongs to the fractal-Gaussian-process-driven Poisson-process family and hence exhibits the fractal characteristics imparted to it by $r(t)$.

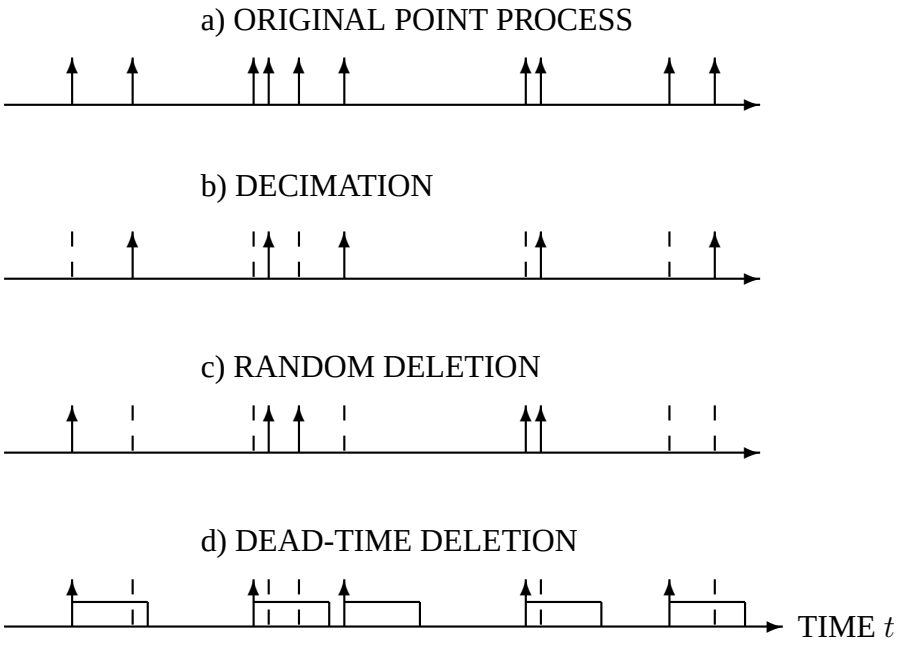

Fig. 11.1 The effect of different types of event deletion on a representative point process. Arrows indicate surviving events; dashed lines indicate deleted events. (a) *Original point process*. (b) *Decimated point process*: Every ℓth event survives, here with $\ell = 2$. (c) *Randomly deleted point process*: Events are randomly deleted, here with survival probability $r = \frac{1}{2}$ so that roughly half of the events survive the deletion process; no particular pattern emerges since each event deletion is independent of the others and of the form of the point process. (d) *Dead-time-modified point process*: We choose a fixed dead time in this illustration so that $r(t)$ switches abruptly from zero to unity at the expiration of the dead-time interval τ_f; the rectangles beginning at each surviving event serve to illustrate the duration of this interval and do not form part of the resulting point process.

the following results do not necessarily apply. The point-process spectrum for a fractal-rate process subjected to dead time is instead provided in Eq. (11.30).

Since the mean rate changes by the factor r, we have $\mathrm{E}[\tau_R] = \mathrm{E}[\tau_1]/r$. Consider the spectrum at a particular frequency f that lies within the scaling range of frequencies. This quantity derives from the squared magnitude of a Fourier transform, so that reducing the number of events to a fraction r of the initial number results in a decrease in the Fourier transform by this same fraction. The spectrum thus changes by the factor r^2 at intermediate frequencies, which provides

$$\begin{aligned} S_{NR}(f) &= r^2 S_{N1}(f) \\ &\approx r^2 \mathrm{E}[\mu_1]\,(f/f_{S1})^{-\alpha_1} \\ &= \mathrm{E}[\mu_R]\,(f/f_{SR})^{-\alpha_1}, \end{aligned} \tag{11.7}$$

with fractal onset frequency $f_{SR} = f_{S1}\, r^{1/\alpha}$.

We conclude that the fractal exponent of the process remains unchanged while the fractal onset *frequency* changes by the factor $r^{1/\alpha}$, which serves to reduce the magnitude of the fractal component. The onset *times* of other second-order measures thus increase by the factor $r^{-1/\alpha}$. At higher frequencies no correlation exists among events in the point process so that the spectrum varies linearly (rather than quadratically) with r, whereupon

$$\lim_{f\to\infty} S_{NR}(f) = \mathrm{E}[\mu_R] = r\mathrm{E}[\mu_1] = r \lim_{f\to\infty} S_{N1}(f). \tag{11.8}$$

11.2.2 Decimation

The deletion of the initial $\ell - 1$ of every ℓ events (retaining every ℓ th event) generally changes the nature of a point process and tends to reduce fluctuations in all measures. The quantity ℓ is known as the **decimation parameter**. We illustrate this operation in Fig. 11.1b) for $\ell = 2$. Consider, for example, a homogeneous Poisson process $dN_1(t)$: in accordance with the results provided in Sec. 4.1, the coefficient of variation of the intervals, $C_\tau = \sqrt{\mathrm{Var}[\tau]}/\mathrm{E}[\tau]$, assumes a value of unity, as does the normalized variance of the counts, $F(T)$, for all counting times T. Retaining the ℓ th, 2ℓ th, 3ℓ th,... events of such a process results in a gamma renewal process of order $\ell = \mathsf{m}$ (see Prob. 4.7 and, for example, Parzen, 1962; Cox, 1962; Cox & Isham, 1980). The coefficient of variation of the intervals becomes $1/\sqrt{\ell}$ whereas the normalized variance $F(T)$ becomes $1/\ell$ for large counting times T. The diminution of both of these quantities indicates that the point process has reduced variability.

Similar results obtain for an arbitrary point process; orderly deletion generally modifies the form of the point process and reduces the fluctuations. Two notable exceptions exist, however. A renewal point process, under decimation, remains within the fold of the renewal-process family despite the fact that it becomes a different process. Integrate-and-reset processes form the second exception. The deletion of the first $\ell - 1$ of every ℓ events in such a process yields results identical to those obtained by decreasing the rate of the process by the same factor ℓ.

For an arbitrary fractal-based point process $dN_1(t)$, decimation leads to a process $dN_R(t)$ that continues to belong to the family of fractal-based point processes, with parameters given by Eq. (11.7) and its associated results, despite possible changes to the form of the point process.

11.2.3 Random deletion

We now consider the consequences of subjecting every event of a point process $dN_1(t)$ to a Bernoulli trial (van der Waerden, 1975), which it survives with probability r or fails to survive with probability $(1 - r)$ (Palm, 1943; Parzen, 1962; Cox & Isham, 1980). We depict this operation in Fig. 11.1c) for $r = \frac{1}{2}$.

The **Burgess variance theorem** (Burgess, 1959) leads to a simple relationship between the normalized count variance for an arbitrary point process and that of its

randomly deleted cousin (Teich & Saleh, 1982):

$$F_R(T) - 1 = r\,[F_1(T) - 1]. \tag{11.9}$$

We can readily extend Eq. (11.9) to the collection of measures set forth in Chapter 3. Beginning with Eq. (3.41), we immediately obtain an analogous relation between the normalized Haar-wavelet variances:

$$A_R(T) - 1 = r\,[A_1(T) - 1]. \tag{11.10}$$

Continuing along these same lines, Eq. (3.55) reveals that the coincidence rate requires multiplication by a factor of r^2, since both $\mathrm{E}[\mu]$ and $F(T) - 1$ decrease by a factor of r, but the delta function at $t = 0$ is subjected only to a factor of r, so that

$$G_R(t) - \mathrm{E}[\mu_R]\,\delta(t) = r^2\big\{G_1(t) - \mathrm{E}[\mu_1]\,\delta(t)\big\}. \tag{11.11}$$

This result, in turn, propagates to the count autocorrelation $R_Z(k, T)$ via Eq. (3.54), which provides

$$R_{ZR}(k, T) - \mathrm{E}[\mu_R]\,T = r^2\big\{R_{Z1}(k, T) - \mathrm{E}[\mu_1]\,T\big\}, \tag{11.12}$$

and to the point-process spectrum $S_N(f)$ through Eq. (3.57), which gives rise to

$$S_{NR}(f) - \mathrm{E}[\mu_R] = r^2\big\{S_{N1}(f) - \mathrm{E}[\mu_1]\big\}. \tag{11.13}$$

Fractal onset times increase by $r^{-1/\alpha}$, and fractal onset frequencies decrease by $r^{1/\alpha}$, maintaining the validity of Eq. (5.45).

As with decimation, random deletion generally alters the nature of a point process. This operation causes the resulting process $dN_R(t)$ to ultimately move toward the homogeneous Poisson process, whatever its original form (Rényi, 1956; Kallenberg, 1975; Wescott, 1976). Random deletion thus serves to reduce the variability of a point process when its fluctuations are greater than those of the benchmark homogeneous Poisson, and to increase the variability for a process whose fluctuations lie below those of the Poisson (Teich & Saleh, 1982). This outcome stands in contrast to that for decimation, which always results in a reduction of variability, as discussed in Sec. 11.2.2.

This tendency toward the homogeneous Poisson process can be observed to some extent in Fig. 11.2, which displays the estimated normalized interevent-interval histogram following random deletion for the seven canonical point processes shown in Fig. 5.9. The retention probability $r = \frac{1}{4}$. In particular, the HEARTBEAT interval histogram, which is quite narrow in Fig. 5.9 by virtue of the clocklike sequence of events comprising the point process, is substantially broadened and displays a nearly exponential form in Fig. 11.2. Nevertheless, examination of the COMPUTER and GENICULATE data reveals that their features are more-or-less conserved under random deletion. In particular, deletion highlights the phase-locked character of the GENICULATE point process by increasing the relative number of interevent intervals at large multiples of the stimulus period (see, for example, Teich et al., 1993, for a discussion of phase locking).

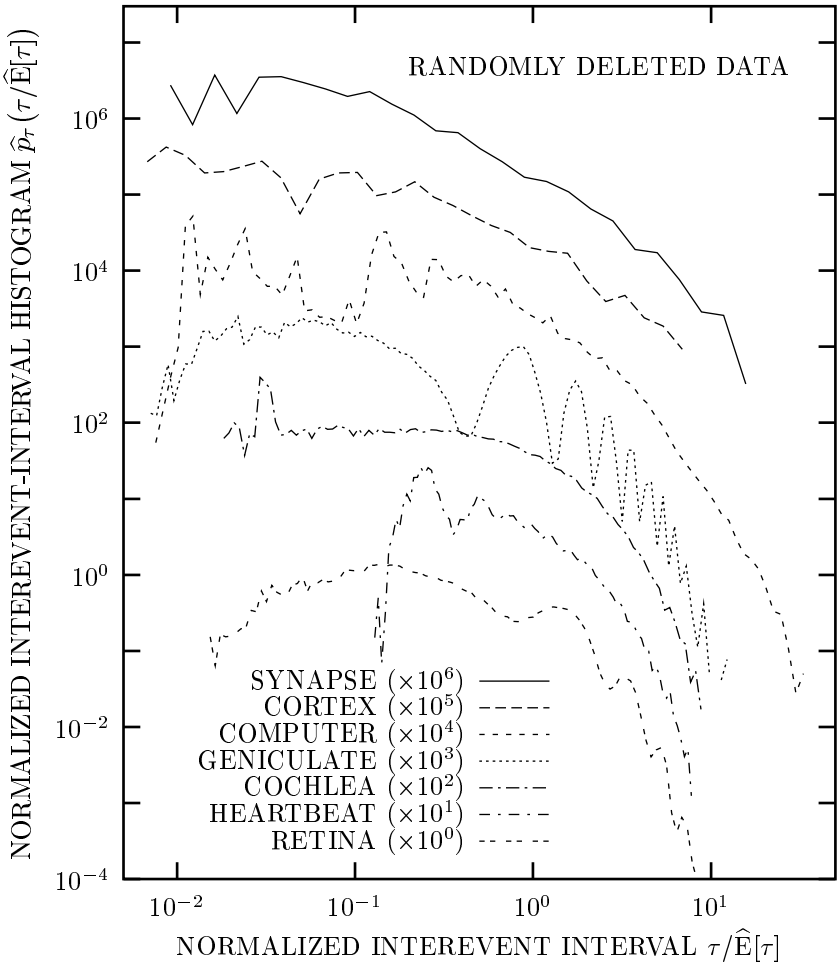

Fig. 11.2 Estimated normalized interevent-interval histogram following random deletion, $\widehat{p}_\tau(\tau/\widehat{\mathrm{E}}[\tau])$ vs. normalized interevent interval $\tau/\widehat{\mathrm{E}}[\tau]$, for the same seven point processes displayed in Fig. 5.9. The retention probability $r = \frac{1}{4}$. We reduced the histogram data to a smaller number of bins for the CORTEX and SYNAPSE data sets because they had only 441 and 688 surviving intervals, respectively. Random deletion ultimately drives point processes toward Poisson form. This can be observed to some extent in the interevent-interval histograms, most noticeably for the HEARTBEAT data. Nevertheless, the principal features of the COMPUTER and GENICULATE data largely remain. In particular, the deletion operation highlights the phase-locked character of the GENICULATE point process.

The perfectly periodic point process $dN_1(t)$, which has interevent intervals $\tau_k = \tau_0$ for all indices k, provides a useful illustration for how random deletion can engender an increase in variability (Teich & Saleh, 1982). The coefficient of variation of the

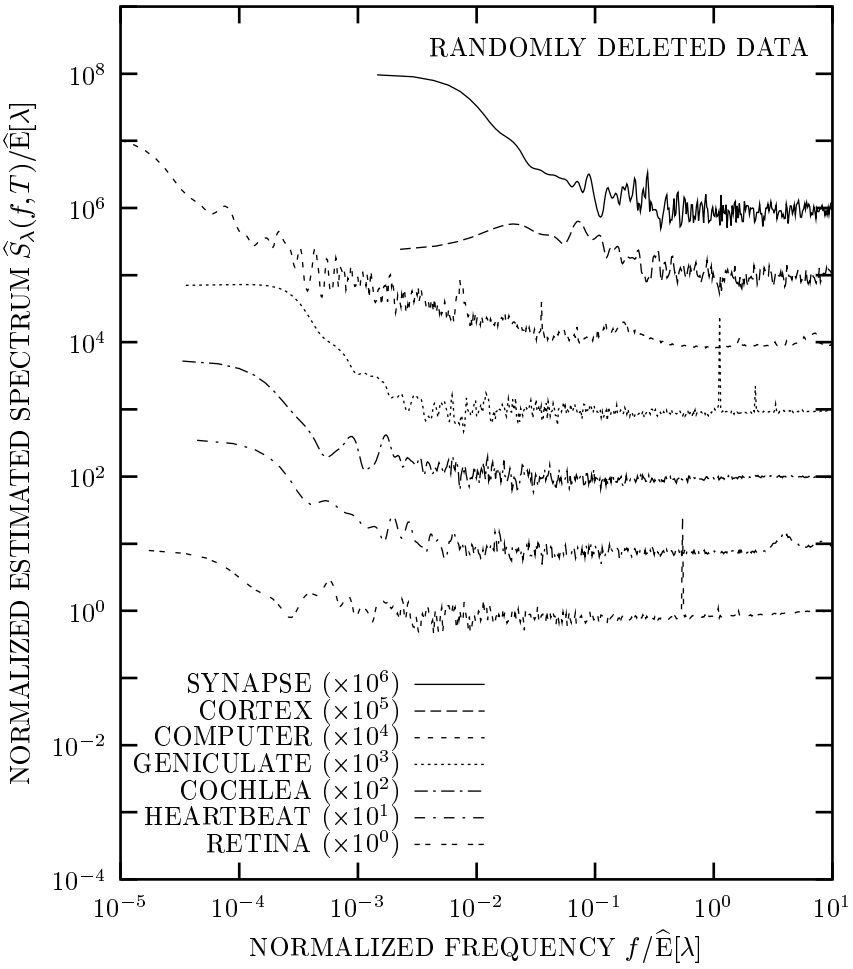

Fig. 11.3 Normalized estimated rate spectra following random deletion, $\widehat{S}_\lambda(f,T)/\widehat{\mathrm{E}}[\lambda]$ vs. normalized frequency $f/\widehat{\mathrm{E}}[\lambda]$, for the six biological point processes and one computer network traffic trace illustrated in Fig. 5.1. The retention probability $r = \frac{1}{4}$. The fractal variability diminishes in magnitude for each of the point processes. The counting time T is chosen such that $1/\sqrt{2} < 30\,T/\mathrm{E}[\tau] < \sqrt{2}$, as it is for all spectra displayed in this chapter, thereby ensuring that the size of the Fourier-transform exceeds the number of intervals by a significant factor $(15\sqrt{2})$.

intervals, $C_\tau = \sqrt{\mathrm{Var}[\tau]}/\mathrm{E}[\tau]$, is of course zero, as is the normalized variance of the counts, $F(T)$, for counting times $T = n\tau_0$ where n is a positive integer. The fact that both of these quantities vanish indicates the absence of randomness in this initial point process. We now subject this process to random deletion by retaining

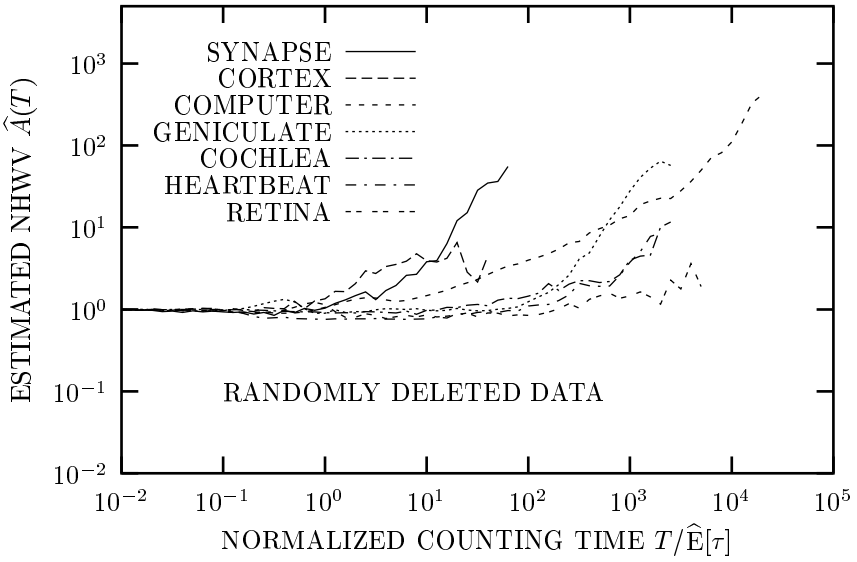

Fig. 11.4 Estimated normalized Haar-wavelet variance (NHWV) following random deletion, $\widehat{A}(T)$ vs. normalized counting time $T/\widehat{\mathrm{E}}[\tau]$, for the same seven point processes as displayed in Fig. 5.2. The retention probability $r = \frac{1}{4}$. As in Fig. 11.3, the fractal variability diminishes in magnitude for each of the point processes.

each event with probability r, independent of the other events and of the time at which the event occurs. The resulting point process $dN_R(t)$, which belongs to the renewal point-process family, obeys

$$\begin{aligned} \Pr\{\tau_R = n\tau_0\} &= r\,(1-r)^{n-1} \\ \Pr\{\tau_R \le n\tau_0\} &= 1-(1-r)^{n} \\ \Pr\{\tau_R \le t\} &= 1-(1-r)^{\mathrm{int}(t/\tau_0)} \\ &= 1-\exp[\mathrm{int}(t/\tau_0)\,\log(1-r)]\,, \end{aligned} \tag{11.14}$$

where $\mathrm{int}(c)$ represents the integer part of the real number c.

In the limit of large values of t/τ_0 and small values of r (signifying that only a small fraction of the events survives), we have $\mathrm{int}(t/\tau_0) \approx t/\tau_0$ and $\log(1-r) \approx -r$, whereupon Eq. (11.14) assumes an exponential form,

$$\begin{aligned} \Pr\{\tau_R \le t\} &\approx 1-\exp(-tr/\tau_0) \\ p_{\tau R}(t) &\approx \big(1/\mathrm{E}[\tau_R]\big)\exp\big(-t/\mathrm{E}[\tau_R]\big), \end{aligned} \tag{11.15}$$

where $\mathrm{E}[\tau_R] = \tau_0/r$, as a result of the properties of the geometric distribution. Since $dN_R(t)$ has an exponentially decaying interevent-interval density, and belongs to the family of renewal point processes, it is, by definition, a homogeneous Poisson

process. Thus, under the influence of heavy random deletion the perfectly periodic integrate-and-reset process becomes a homogeneous Poisson process. The coefficient of variation of the intervals, C_τ, and the normalized variance of the counts, $F(T)$, grows from zero to unity, which unequivocally demonstrates that a substantial increase in variability can be introduced by the operation of random deletion.

As indicated in Sec. 11.2.1, and implicit in the results derived above, random deletion reduces the magnitude of the fractal variability inherent in a point process; this operation converts an arbitrary original fractal-based point process $dN_1(t)$ into its deleted cousin $dN_R(t)$ via Eq. (11.7) and associated formulas. Figures 11.3 and 11.4 demonstrate this reduction for the rate spectra and normalized Haar-wavelet variances, respectively, associated with the canonical data sets displayed in Figs. 5.1 and 5.2. The reduction agrees with the analytical results provided in Eqs. (11.13) and (11.10), respectively.

Two exceptions exist to this rule, whereby random deletion does not change the character of a point process. A renewal point process retains its renewal form under random deletion, although it becomes a different renewal process (see Prob. 11.9). And a doubly stochastic Poisson process remains a doubly stochastic Poisson process (Teich & Saleh, 1982).

11.2.4 Dead-time deletion

In the presence of **dead time**, called **refractoriness** in the biological literature, the probability of event deletion depends on the history of the point process in a more complex manner than it does for decimation. In its most general form, dead-time deletion invokes the history all event occurrences prior to the event at hand. Treating this general problem turns out to be quite unwieldy, however, so that it is common to consider dead-time-deletion models that reach back only to the previous n events (nth-order dead time). Typically, $n = 1$ or 2.

In the following, we consider only first-order dead time ($n = 1$), also known as "one-memory dead time." This case further divides into two types: one in which the surviving process $dN_R(t)$ depends on the last event of the original process $dN_1(t)$ (**paralyzable dead time** or **extended dead time**), and one in which $dN_R(t)$ depends on the last event of the output process $dN_R(t)$ (**nonparalyzable dead time** or **nonextended dead time**).[6] Both types of dead time belong to the more general family of **type-*p* dead time** (Albert & Nelson, 1953; Parzen, 1962; Bharucha-Reid, 1997). An enormous body of literature exists on dead-time effects, and Müller compiled a rather remarkable bibliography on the topic in 1981.

We focus on nonparalyzable dead time, by far the most prevalent form encountered in physical and biological systems. The probability of survival of an event in $dN_1(t)$,

[6] There is a further division, depending on whether the counter is in a "blocked" ("ordinary"), "unblocked" ("shifted" or "free"), or "equilibrium" ("stationary") state at the beginning of the counting duration (see, for example, Müller, 1973, 1974; Libert, 1976). The various results differ minimally when the mean number of events recorded during a sampling time is much greater than unity (Libert, 1976).

which depends only on the time to the last event in $dN_R(t)$, is specified by the so-called **recovery function** $r(t)$. In the special case of **fixed dead time** (called **absolute refractoriness** in the biological literature), $r(t)$ follows the form of a step function:

$$r(t) = \begin{cases} 0 & t < \tau_f \\ 1 & t \geq \tau_f, \end{cases} \tag{11.16}$$

where τ_f is the dead-time period. The deletion of events subjected to fixed dead time is illustrated in Fig 11.1d). More generally, **relative dead time** (known as **relative refractoriness** in the biological literature) occurs, whereupon $r(t)$ assumes a more general form. Relative dead time is also descriptively referred to as **sick time** (Teich & Diament, 1980). Yet another variation on the theme involves **stochastic dead time**, in which the dead time is absolute but random (see, for example, Cantor, Matin & Teich, 1975; Teich et al., 1978).

Even with these simplifications, general results are difficult to obtain. We therefore further limit ourselves to a few particular cases that serve as useful models for the kinds of dead-time effects often encountered in point processes and that prove amenable to analysis. In particular, we consider (1) general point processes modified by fixed nonparalyzable dead time; (2) homogeneous Poisson processes modified by relative nonparalyzable dead time; (3) Poisson-based processes modified by relative nonparalyzable dead time; and (4) integrate-and-reset processes modified by relative nonparalyzable dead time.

- The imposition of **fixed dead time** on a **general point process** closely resembles the minimal-covering procedure used to calculate the capacity dimension in Sec. 7.2.5 (see Fig 7.7). Indeed, the same formalism yields a general result for the mean interevent time. For a general point process, we again make use of Wald's Lemma (Feller, 1971) to obtain the expected value of the time between events in the resulting point process,

  $$E[\tau_R] = \mathrm{E}^2[\tau_1] \int_{0-}^{\tau_f} G_1(t)\, dt. \tag{11.17}$$

  The quantity $G_1(t)$ denotes the coincidence rate of the point process $dN_1(t)$, and the notation $0-$ indicates that the range of integration spans the delta function in $G_1(t)$ at $t = 0$. Examples of point processes in this class have been considered by Cantor & Teich (1975); Teich & McGill (1976); Teich & Vannucci (1978); Vannucci & Teich (1978, 1981); Saleh et al. (1981); and Prucnal & Teich (1983).

- We next consider the **dead-time-modified homogeneous Poisson process**, which has a broad range of applicability in many fields of endeavor. The fixed-dead-time version of this process has a long history in the annals of probability (Morant, 1921; Palm, 1943; Jost, 1947; Parzen, 1962; DeLotto, Manfredi & Principi, 1964; Müller, 1973; Cantor & Teich, 1975; Müller, 1981). Feller (1948) provided an early comprehensive analysis. As a result of the absence of

memory in the original process $dN_1(t)$, the dead-time deleted version, $dN_R(t)$, is renewal in nature.

Following the occurrence of an event in $dN_R(t)$, the effective rate $\mu_R(t)$ of $dN_R(t)$ simply becomes $\mu_1 r(t)$. The probability of zero events occurring in $dN_R(t)$ between an event and a later time t, which is equivalent to the survivor function $1 - P_{\tau R}(t)$ of $dN_R(t)$, decays as an exponential transform of the integrated rate, as shown in Eqs. (4.26) and (4.28):

$$1 - P_{\tau R}(t) = \exp\left[-\mu_1 \int_0^t r(u)\, du\right]. \tag{11.18}$$

The mean interevent time for the resulting point process is obtained from Eq. (11.18):

$$\begin{aligned} \mathrm{E}[\tau_R] &= \int_0^\infty t p_{\tau R}(t)\, dt \\ &= \int_0^\infty [1 - P_{\tau R}(t)]\, dt \qquad (11.19) \\ &= \int_0^\infty \exp\left[-\mu_1 \int_0^t r(u)\, du\right]\, dt, \qquad (11.20) \end{aligned}$$

where Eq. (11.19) follows from integration by parts and resembles Eq. (3.11) for $s \to \infty$.

We define an effective dead time τ_e as the difference between the mean interevent intervals for the two processes,

$$\tau_e \equiv \mathrm{E}[\tau_R] - \mathrm{E}[\tau_1] = \mathrm{E}[\tau_R] - 1/\mu_1. \tag{11.21}$$

Rearranging Eq. (11.21) yields the expectation of the effective rate,

$$\begin{aligned} \mathrm{E}[\tau_R] &= 1/\mu_1 + \tau_e = 1/\mathrm{E}[\mu_R] \\ \mathrm{E}[\mu_R] &= \frac{\mu_1}{1 + \mu_1\, \tau_e}. \end{aligned} \tag{11.22}$$

- More generally, we examine the **dead-time-modified driven Poisson process**. Suppose that the initial point process $dN(t)$ maintains its Poisson character but has a varying rate $\mu_1(t)$, as considered by Vannucci & Teich (1978, 1981). We assume that $\mu_1(t)$ varies slowly in comparison with the mean interevent time of the resulting process, $\mathrm{E}[\tau_R]$, and that the standard deviation of $\mu_1(t)$ is much smaller than its mean. The instantaneous rate then follows the form of Eq. (11.22) without the expectation,

$$\mu_R(t) = \frac{\mu_1(t)}{1 + \mu_1(t)\tau_e}. \tag{11.23}$$

To simplify the ensuing algebra, we define two functions,

$$\begin{aligned} x(t) &\equiv 1 + \mu_1(t)\,\tau_e \\ y(t) &\equiv \frac{x(t) - \mathrm{E}[x]}{\mathrm{E}[x]}, \end{aligned} \tag{11.24}$$

whereupon

$$\begin{aligned} \mu_R(t)\,\tau_e &= \frac{\mu_1(t)\,\tau_e}{1 + \mu_1(t)\,\tau_e} \\ &= 1 - \frac{1}{1 + \mu_1(t)\,\tau_e} \\ &= 1 - \frac{1}{x(t)} \\ &= 1 - \frac{1}{x(t) - \mathrm{E}[x] + \mathrm{E}[x]} \\ &= 1 - \frac{1}{\mathrm{E}[x]}\,\frac{1}{1 + y(t)} \\ &= 1 - \frac{1}{\mathrm{E}[x]} \sum_{n=0}^{\infty} [-y(t)]^n. \end{aligned} \tag{11.25}$$

The convergence of the power series in Eq. (11.25) follows from the assumed small value of $y(t)$, which, in turn, derives from the small degree of relative fluctuations in $\mu_1(t)$. Retaining terms to second order in this perturbation analysis leads to

$$\begin{aligned} \mu_R(t)\,\tau_e &\approx 1 - \frac{1}{\mathrm{E}[x]}\left[1 - y(t) + y^2(t)\right] \\ &= 1 - \frac{1}{\mathrm{E}[x]} + \frac{x(t) - \mathrm{E}[x]}{\mathrm{E}^2[x]} - \frac{\left\{x(t) - \mathrm{E}[x]\right\}^2}{\mathrm{E}^3[x]} \\ \mu_R(t) &\approx \frac{\mathrm{E}[\mu_1]}{1 + \mathrm{E}[\mu_1]\,\tau_e} + \frac{\mu_1(t) - \mathrm{E}[\mu_1]}{\left(1 + \mathrm{E}[\mu_1]\,\tau_e\right)^2} - \tau_e \frac{\left\{\mu_1(t) - \mathrm{E}[\mu_1]\right\}^2}{\left(1 + \mathrm{E}[\mu_1]\,\tau_e\right)^3}. \end{aligned} \tag{11.26}$$

Finally, forming the expectation of Eq. (11.26) leads to a second-order approximation for the mean rate,

$$\mathrm{E}[\mu_R] \approx \frac{\mathrm{E}[\mu_1]}{1 + \mathrm{E}[\mu_1]\,\tau_e} - \frac{\mathrm{Var}[\mu_1]\,\tau_e}{\left(1 + \mathrm{E}[\mu_1]\,\tau_e\right)^3}. \tag{11.27}$$

More exact results are available for the specific case when $r(t)$ takes the form of a delayed exponential function (Lowen, 1996).

In preparation for computing the autocovariance, we rearrange Eq. (11.27) to provide

$$\mu_R - \mathrm{E}[\mu_R] \approx \frac{\mu_1(t) - \mathrm{E}[\mu_1]}{\left(1 + \mathrm{E}[\mu_1]\,\tau_e\right)^2} - \tau_e \frac{\left\{\mu_1(t) - \mathrm{E}[\mu_1]\right\}^2 - \mathrm{Var}[\mu_1]}{\left(1 + \mathrm{E}[\mu_1]\,\tau_e\right)^3}. \quad (11.28)$$

The second fraction in Eq. (11.28) becomes insignificant when calculating the autocovariance, however, since it only appears in third- and higher-order terms; we thus obtain (Lowen, 1996)

$$\begin{aligned} \mathrm{E}\Big[\left\{\mu_R(s) - \mathrm{E}[\mu_R]\right\}\left\{\mu_R(s+t) - \mathrm{E}[\mu_R]\right\}\Big] & \\ \approx \mathrm{E}\left\{ \frac{\mu_1(s) - \mathrm{E}[\mu_1]}{\left(1 + \mathrm{E}[\mu_1]\,\tau_e\right)^2} \cdot \frac{\mu_1(s+t) - \mathrm{E}[\mu_1]}{\left(1 + \mathrm{E}[\mu_1]\,\tau_e\right)^2} \right\} & \\ R_{\mu R}(t) - \mathrm{E}^2[\mu_R] \approx \left(\mathrm{E}[\mu_R]/\mathrm{E}[\mu_1]\right)^4 \left\{R_{\mu 1}(t) - \mathrm{E}^2[\mu_1]\right\}. & \quad (11.29) \end{aligned}$$

Pursuing the formalism provided in Eq. (11.7) then leads to

$$\begin{aligned} S_{NR}(f) &\approx \left(\mathrm{E}[\mu_R]/\mathrm{E}[\mu_1]\right)^4 S_{N1}(f) \\ &= \left(\mathrm{E}[\mu_R]/\mathrm{E}[\mu_1]\right)^4 \mathrm{E}[\mu_1]\,(f/f_{S1})^{-\alpha} \\ &= \mathrm{E}[\mu_R]\,(f/f_{SR})^{-\alpha}, \end{aligned} \quad (11.30)$$

with fractal onset frequency $f_{SR} = f_{S1}(\mathrm{E}[\mu_R]/\mathrm{E}[\mu_1])^{3/\alpha}$. This result contrasts with that provided just after Eq. (11.7) for random deletion, which is $f_{SR} = f_{S1}(\mathrm{E}[\mu_R]/\mathrm{E}[\mu_1])^{1/\alpha}$. The distinction arises because dead time preferentially deletes closely spaced intervals relative to sparsely populated ones. This serves to reduce high rates more than low rates and thereby reduces the fluctuations in the rate. This, in turn, leads to a more regular process than would emerge by deletion of the same number of events without regard to the event timings. Hence, given the same initial point process, dead-time-modified processes tend to have lower fractal onset frequencies (and higher fractal onset times) than randomly deleted processes of the same rate. The relationships in Eq. (5.45) remain valid since the cutoff time T_A (as well as T_F, t_G, and T_R for $\alpha < 1$) increases by the inverse factor, namely $(\mathrm{E}[\mu_R]/(\mathrm{E}[\mu_1])^{-3/\alpha}$.

Dead time effects are principally short term while fractal effects are most important in the long term, so they conveniently decouple, at least for the doubly stochastic Poisson process. We can readily incorporate the two effects into a single formula by using the dead-time factor $(1 + \mathrm{E}[\mu]\tau_e)^3$ in conjunction with the fractal term, and adding in the dead-time result. As an example, let $A_1(T)$ denote the normalized Haar-wavelet variance for a dead-time-modified homogeneous Poisson process, and $A_2(T)$ denote the normalized Haar-wavelet variance for a fractal doubly stochastic Poisson process without dead time. The overall normalized Haar-wavelet variance $A_3(T)$ then becomes (Lowen, 1996)

$$A_3(T) = A_1(T) + (1 + \mathrm{E}[\mu]\tau_e)^3\,[A_2(T) - 1]. \quad (11.31)$$

- Finally we turn to the **dead-time-modified integrate-and-reset process**. For a constant rate μ_1, we again have $\mu_R(t) = \mu_1 r(t)$, but in this case Eq. (4.35) provides

$$\begin{aligned} \int_0^{\tau_R} \mu_R(t)\,dt &= \mu_1 \int_0^{\tau_R} r(t)\,dt = 1 \\ \int_0^{\tau_R} r(t)\,dt &= \tau_1 \\ r(\tau_R) &= d\tau_1/d\tau_R. \end{aligned} \tag{11.32}$$

Following the procedure used earlier, but now for the integrate-and-reset process, we obtain

$$\begin{aligned} \mu_R(t) &\approx \mathrm{E}[\mu_R] + \frac{d\mu_R}{d\mu_1}\left\{\mu_1(t) - \mathrm{E}[\mu_1]\right\}^2 \\ R_{\mu R}(t) - \mathrm{E}^2[\mu_R] &\approx \left(\frac{d\mu_R}{d\mu_1}\right)^2 \left\{R_{\mu 1}(t) - \mathrm{E}^2[\mu_1]\right\}. \end{aligned} \tag{11.33}$$

We calculate the derivative in Eq. (11.33) with the help of Eq. (11.32), which gives rise to

$$\begin{aligned} \frac{d\mu_R}{d\mu_1} &= \frac{d(1/\tau_R)}{d\mu_1} = -\tau_R^{-2}\frac{d\tau_R}{d\mu_1} = -\tau_R^{-2}\left[\frac{d\mu_1}{d\tau_R}\right]^{-1} \\ &= -\tau_R^{-2}\left[\frac{d(1/\tau_1)}{d\tau_R}\right]^{-1} = -\frac{1}{\tau_R^2}\left[-\frac{r(\tau_R)}{\tau_1^2}\right]^{-1} \\ &= \left(\mu_R/\mu_1\right)^2 r^{-1}(\tau_R). \end{aligned} \tag{11.34}$$

Finally, combining Eqs. (11.33) and (11.34) yields

$$R_{\mu R}(t) - \mathrm{E}^2[\mu_R] \approx \left(\mathrm{E}[\mu_R]/\mathrm{E}[\mu_1]\right)^4 r^{-2}\big(\mathrm{E}[\tau_R]\big)\left\{R_{\mu 1}(t) - \mathrm{E}^2[\mu_1]\right\}. \tag{11.35}$$

In particular, for fixed dead time, as specified in Eq. (11.16), we have $r(\tau_R) = 1$ for all possible τ_R, which yields results identical to those provided in Eq. (11.29), and thus also to those given in Eq. (11.30). In general, for integrate-and-reset deletion processes the changes in fractal onset times and frequencies depend on the form of $r(t)$.

11.3 DISPLACEMENT

The **displacement** operation, sometimes called **translation**, signifies a shifting of the individual events of a point process, typically by a random amount (Cox, 1963).

Random jitter results in a loss of phase coherence, so it can mask features of interest in the unmodified point process. Although the magnitude of the displacement can in principle be made to depend on a variety of properties of the point process, such as its local mean rate or some complex function of its history (Harris, 1971), constructs of this kind have limited usefulness and are difficult to analyze. Rather, we focus on two simple approaches to displacement, based on the intervals between events and on the events themselves, respectively.

11.3.1 Interval displacement

In the displaced-interval approach, each interevent interval is multiplied by a random quantity that is close to unity, such as

$$\tau_{kR} = \tau_{k1}\Big[1 + \sigma\mathcal{N}_k(0,1)\Big] \tag{11.36}$$

where σ is the dimensionless relative scale of the displacement (akin to a standard deviation) and $\{\mathcal{N}_k(0,1)\}$ is a sequence of independent, zero-mean, unity-variance Gaussian random variables (Thurner et al., 1997). Typically we choose $\sigma \ll 1$ so that, with rare exception, $\tau_{kR} > 0$.

Rather than relying on multiplication, we could instead add a random value to each interevent interval, for example via

$$\tau_{kR} = \tau_{k1} + \sigma\mathcal{N}_k(0,1)\,\mathrm{E}[\tau_{k1}]. \tag{11.37}$$

We have not found the additive approach to be useful, however, because it either requires very small values of σ (in which case large values of τ_{kR} experience little change) or it leads to many negative values of τ_{k1}.

For displacement, as specified in either Eq. (11.36) or (11.37), we can rectify the problem of negative τ_{k1} in a number of ways; we specify two. The first approach involves specifying a minimum interevent interval, and replacing all values inferior to it with that minimum value. Alternatively, we can reorder the events t_{kR} in the resulting point process so that the intervals all become positive, but this approach introduces additional complexity. For any method, displacing the intervals yields a new point process that precisely preserves the number of interevent intervals in the original process, but not its duration.

11.3.2 Event-time displacement

In the displaced event-time approach, we add a random quantity to each event time so that, for example,

$$t_{kR} = t_{k1} + \sigma\mathcal{N}_k(0,1)\,\mathrm{E}[\tau_{k1}], \tag{11.38}$$

where the definitions of σ and $\{\mathcal{N}_k(0,1)\}$ are given in conjunction with Eqs. (11.36) and (11.37). Note that this differs from Eq. (11.37). Multiplication by a random value, as formulated in Eq. (11.36), is not viable in this case since it leads to increasingly larger displacements as t increases. Again, we can set $\Pr\{\tau_{k1} < \sigma\mathrm{E}[\tau_{k1}]\} \ll 1$ so

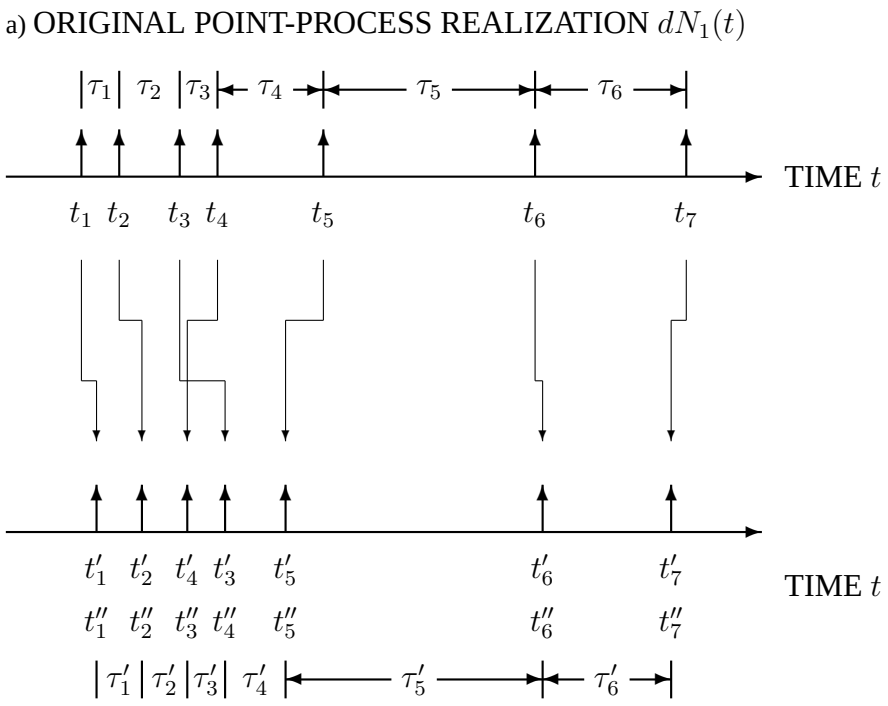

Fig. 11.5 Original and displaced point-process realizations. (a) An original point process realization $dN_1(t)$ comprises seven event times $\{t_k\}$ and six concomitant interevent intervals $\{\tau_k\}$. A random displacement of the event times $\{t_k\}$ in the original realization shown in a) yields a new set of event times $\{t'_k\}$; after reordering in increasing temporal order, these become the event times $\{t''_k\}$ of the displaced realization shown in b). The six interevent intervals $\{\tau'_k\}$ of this displaced realization derive from the relation $\tau'_k = t''_{k+1} - t''_k$. In general the start times differ ($t'_1 \neq t_1$), in contrast to the outcome for interval shuffling (Sec. 11.5).

that $\tau_{kR} > 0$ with only rare exception, and then set a minimum interevent interval; sort t_{kR} into increasing order; or use a combination of these methods to ensure that τ_{kR} does not assume negative values.

A schematic illustration of displacing the event times of a point process appears in Fig. 11.5. Event displacement yields a new point process that exactly preserves the number of interevent intervals in the original process, and also closely preserves its duration. In general, both methods (with reordering, if required) destroy whatever structure might have been present in the original point process $dN_1(t)$ at time scales smaller than $\sigma \mathrm{E}[\tau_{k1}]$, replacing it with (locally) homogeneous-Poisson behavior at those scales. To understand how this comes about, consider a fractal-Gaussian-process-driven integrate-and-reset process $dN_1(t)$. Now apply the transformation

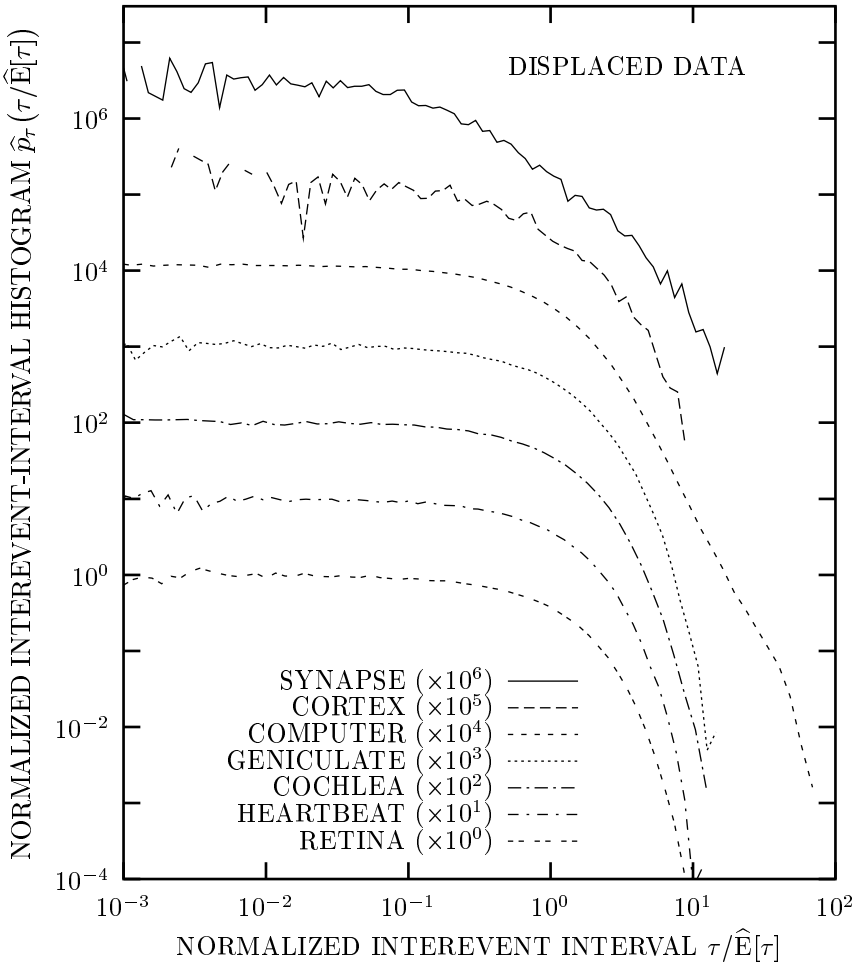

Fig. 11.6 Estimated normalized interevent-interval histogram following random displacement, $\widehat{p}_\tau(\tau/\widehat{\mathrm{E}}[\tau])$ vs. normalized interevent interval $\tau/\widehat{\mathrm{E}}[\tau]$, for the same seven point processes displayed in Fig. 5.9. We add a random value to each event time in the data set. These values are drawn from a zero-mean Gaussian-distributed distribution with a standard deviation equal to ten times the mean interevent interval of the data set under study. All random variables are independent of each other. We reduced the histogram data to the same number of bins (namely 100) for all data sets. Most of the curves assume a form that is essentially exponential, confirming that the structure in the original histograms reflects the existence of particular interval orderings over short time scales.

of Eq. (11.38) with a large value of σ, such as 10; each event then experiences a random shift of the order of $10\mathrm{E}[\tau_{k1}]$. In particular, the integrate-and-reset character of the point process does not survive in the resulting process $dN_R(t)$. However,

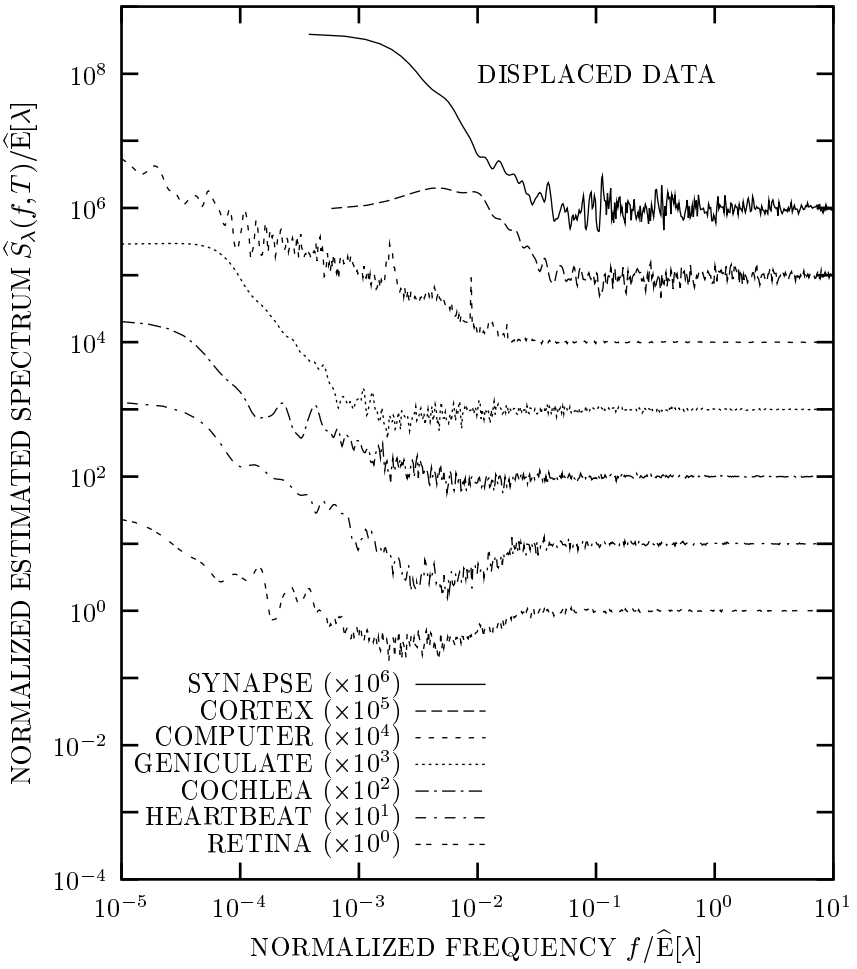

Fig. 11.7 Normalized estimated spectra following random displacement, $\widehat{S}_\lambda(f,T)/\widehat{\mathrm{E}}[\lambda]$ vs. normalized frequency $f/\widehat{\mathrm{E}}[\lambda]$, for the six biological point processes and one computer network traffic trace illustrated in Fig. 5.1. We add a random value to each event time in the data set. These values are drawn from a zero-mean Gaussian-distributed distribution with a standard deviation equal to ten times the mean interevent interval of the data set under study. All random variables are independent of each other. This operation eliminates all structure at high frequencies for all of the point processes, whereas the fractal variability at low frequencies remains intact.

fractal behavior, and indeed all long-term fluctuations, suffer little change so that the statistics of $dN_R(t)$ closely resemble those of $dN_1(t)$ over time scales significantly greater than $10\mathrm{E}[\tau_{k1}]$.

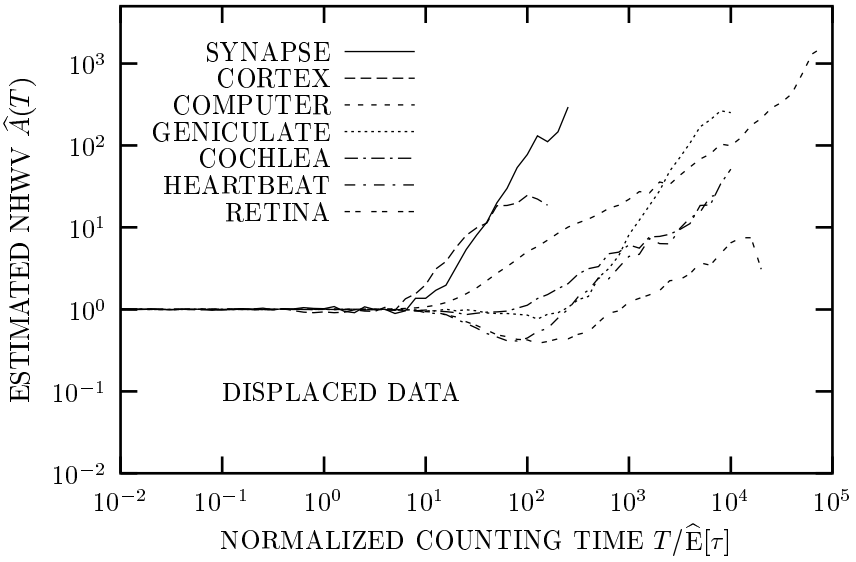

Fig. 11.8 Estimated normalized Haar-wavelet variance (NHWV) following random displacement, $\widehat{A}(T)$ vs. normalized counting time $T/\widehat{\mathrm{E}}[\tau]$, for the same seven point processes as displayed in Fig. 5.2. We add a random value to each event time in the data set. The values are drawn from a zero-mean Gaussian-distributed distribution with a standard deviation equal to ten times the mean interevent interval of the data set under study. All random variables are independent of each other. This operation eradicates all structure at small values of the normalized counting time for all of the point processes, whereas the fractal variability at large values of the normalized counting time remains intact.

We now proceed to establish the Poisson character of $dN_R(t)$ over small times scales. Consider a large number n of adjacent counting intervals of short duration T, such that $nT/10\mathrm{E}[\tau_{k1}] \ll 1$. The displacements, which greatly exceed the duration of the counting intervals nT, ensure that the resulting counts $Z_k(T)$ are independent and identically distributed, given the same overall local rate. In the limit as $T \to 0$ with nT fixed, the counts $Z_k(T)$ approach independent Bernoulli random variables with identical properties. This satisfies Eqs. (4.1) and (4.2), indicating that the point process $dN_R(t)$ over this interval nT becomes identical to a homogeneous Poisson process.

Under these conditions, the interevent-interval histogram approaches an exponential form. The results presented in Fig. 11.6 are, indeed, close to exponential. This is not unexpected since the events are shifted by Gaussian random numbers with zero mean and standard deviations equal to ten times the mean interevent interval. Locally, then, the process is nearly Poisson. The aggregate displaced interevent-interval histogram should then become the original histogram smeared by an exponential. If the rate remains relatively constant, as it is for the lower four data sets displayed in

Fig. 11.6, the smearing process obliterates all traces of the original interevent-interval histogram, leaving essentially a pure exponential in its place. On the other hand, if the rate exhibits large variations, some regions of the point processes will be dominated by short intervals while other regions will be dominated by long ones. The interevent-interval histogram will then deviate from an exponential form, especially for the larger intervals. This occurs in the upper three data sets displayed in Fig. 11.6 because of the wide variation in their rates. The deviation from exponential form is particularly apparent for the COMPUTER data because it has nearly a thousand times as many intervals as the SYNAPSE and CORTEX data, thereby making the effect more apparent.

In Figs. 11.7 and 11.8 we illustrate the effects of event-time displacement, implemented according to the prescription provided in Fig. 11.5, on the spectra and normalized Haar-wavelet variances of the canonical set of point processes shown in Figs. 5.1 and 5.2. The fractal behavior at low frequencies (large values of the normalized counting time) remains intact; however, all structure at high frequencies (small values of the normalized counting time) is eliminated and the process becomes Poisson-like, as evidenced by the fact that $\widehat{A}(T) = 1$ in this range.

11.4 INTERVAL TRANSFORMATION

We turn now to interval transformation, in which the relative ordering of the interevent intervals remains unchanged but their overall probability distribution is modified. This operation creates a surrogate data set testing the hypothesis that behavior in a particular measure derives from the interevent-interval distribution.

Figure 11.9 illustrates the procedure of interval transformation. This procedure maintains the ordering of the set of interevent intervals $\{\tau_n\}$, but each interval is resized by drawing it from an arbitrary probability distribution. Like displacement, interval transformation yields a new point process that exactly preserves the number of interevent intervals in the original process, and also closely preserves its duration. However, the particular original point process realization illustrated in Fig. 11.9 has interevent intervals that exhibit a relatively low coefficient of variation; the interval-transformed realization has a greater proportion of smaller and larger intervals at the expense of values near the mean. The nature of the point process has changed. A simple method for carrying out this transformation on a set of M interevent intervals includes the following five steps[7] (steps 3 and 4 can precede steps 1 and 2 to save memory):

[7] Alternatively, one could construct a monotonically increasing function and apply it to each interevent interval τ_n in the original realization to generate the corresponding interval in the new realization, choosing a form for the function that yields the correct empirical fit for the distribution of $\{\tau_n'\}$. However, aside from requiring intervention tailored to each data set, this procedure does not admit more than one possible realization. Randomness is not present in the generated realization in this case.

1. Generate M independent random numbers with the desired distribution, and call this array $\{\tau'_n\}$.
2. Sort $\{\tau'_n\}$ into ascending order.
3. Generate an auxiliary array of integers in ascending order, ranging from 1 to M, and call this array $\{k_n\}$. Thus, $k_n = n$ at this point.
4. Sort the original array $\{\tau_n\}$ into ascending order, and perform the same operations on the auxiliary array $\{k_n\}$.
5. Sort the auxiliary array $\{k_n\}$ back into ascending order, and perform the same operations on the generated array $\{\tau'_n\}$.

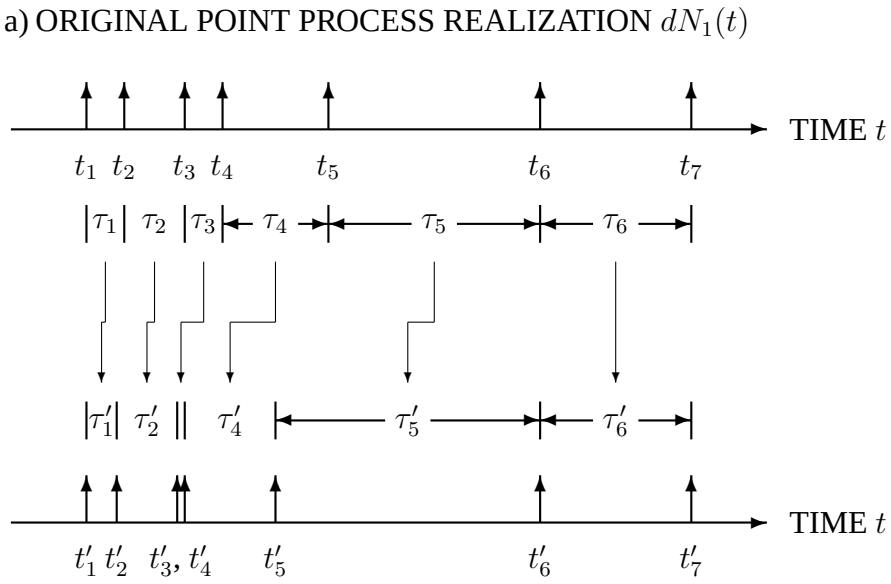

Fig. 11.9 Interval-transformed point process. (a) The original point-process realization has seven event times $\{t_n\}$ and therefore six interevent intervals $\{\tau_n\}$. We replace each interevent interval τ_n with a new random variable drawn from a predetermined distribution (for example, exponential), and preserve the relative ordering of the intervals. This yields the interevent intervals $\{\tau'_n\}$ of the interval-transformed realization (b). As with the interval-transformed realization, the two realizations share the same start time ($t'_1 = t_1$). We then employ the relation $\tau'_n = t'_{n+1} - t'_n$ to yield the seven event times $\{t'_n\}$ of the interval-transformed realization. The label for the interevent interval τ'_3 has been omitted because of lack of space.

11.4.1 Interval normalization

Distribution transformation has long been applied to interval and count data because it confers a number of benefits[8] (Tukey, 1957; Kendall & Stuart, 1966). The principal goals of such transformations are generally to stabilize the variance so that conventional analysis measures can be used (Prucnal & Teich, 1980); convert nonadditive noise into additive form so that well-established detection/estimation techniques apply (Prucnal & Saleh, 1981); and to cast the distribution into a symmetrical form for ease of calculation. A transformation suitable for effecting one of these features often turns out to effect the others as well (Tukey, 1957). Most often, the transformation is to a Gaussian distribution by virtue of the extensive body of available results; it is then called a **normalizing transformation**.

11.4.2 Interval exponentialization

We now consider the effects of transforming the intervals to an exponential distribution, which we term **exponentialization**. In Figs. 11.10 and 11.11, we illustrate the consequences of carrying out this operation on the spectra and normalized Haar-wavelet variances of the canonical set of point processes shown in Figs. 5.1 and 5.2. (We do not display exponentialized interevent-interval histograms since they are exponential by construction.)

To understand the role played by exponentialization, we consider the fractal-Gaussian-process-driven Poisson process described in Sec. 6.3.3. When the coefficient of variation of the rate is small in comparison with unity ($C_\mu \ll 1$), the rate does not depart significantly from its mean value; in particular, it remains nearly constant over times corresponding to a few interevent intervals. Under these conditions, as shown in Eq. (4.33), the interevent-interval density for this process closely follows an exponential form,[9] modulated only minimally by the range of rate values (compare with the argument in Sec. 11.3.2). The sequence of events then closely resembles a homogeneous Poisson process over those time scales. The interval distribution therefore does not contribute to the fractal characteristics of this process; rather, this behavior arises from the ordering of the intervals. Hence, one method for testing whether the interval distribution induces fractal behavior in a point process involves

[8] Approximate normalizing transformations do, in fact, exist for nonparalyzable and paralyzable dead-time-modified Poisson counting systems (Teich, 1985).

[9] The sequence of action potentials generated in primary afferent auditory nerve fibers, either firing spontaneously or stimulated by high-frequency tones, is well described by a dead-time-modified form of this point process (Teich et al., 1990; Lowen & Teich, 1997). The observation of an interevent-interval density described by a delayed exponential, while ignoring other statistics of the point process, has often led researchers to the (improper) conclusion that the action potentials follow a dead-time-modified homogeneous Poisson process (see, for example, Kiang, Watanabe, Thomas & Clark, 1965, Chapter 8); for a discussion of this issue, see Teich & Khanna (1985); Teich (1992); Lowen & Teich (1992a); Teich & Lowen (1994). Indeed, any number of distinctly non-Poisson point processes can be constructed with exponential interevent-interval densities (see, for example, Moran, 1967; Lawrance, 1972; Glass & Mackey, 1988).

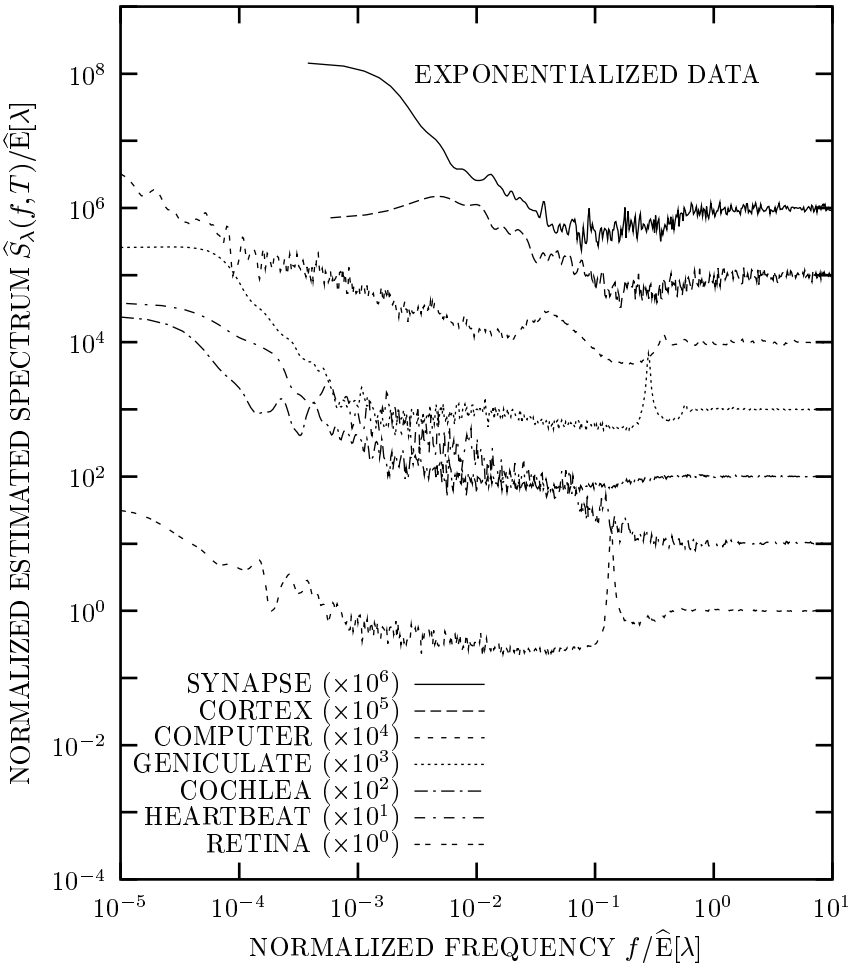

Fig. 11.10 Normalized estimated spectrum after exponentialization, $\widehat{S}_\lambda(f,T)/\widehat{\mathrm{E}}[\lambda]$ vs. normalized frequency $f/\widehat{\mathrm{E}}[\lambda]$, for the six biological point processes and one computer network traffic trace illustrated in Fig. 5.1. There is a substantial reduction of structure at high frequencies for all of the point processes while the fractal variability at low frequencies remains essentially intact or, in the case of the HEARTBEAT point process, is enhanced.

replacing the intervals of the original realization with ones having an exponential form and observing whether the fractal characteristics change.

By way of example, consider a point-process realization exhibiting fractal behavior that depends on both the relative ordering *and* the distribution of the interevent intervals; the fractal-lognormal-noise-driven Poisson process described in Sec. 6.5 behaves in this way. Exponentialized realizations for this process yield results in

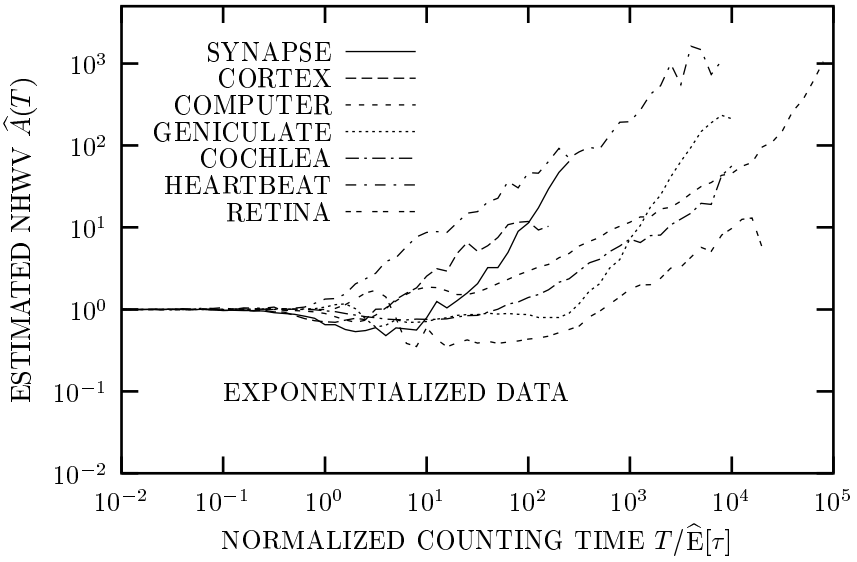

Fig. 11.11 Estimated normalized Haar-wavelet variance (NHWV) following exponentialization, $\widehat{A}(T)$ vs. normalized counting time $T/\widehat{\mathrm{E}}[\tau]$, for the same seven point processes as displayed in Fig. 5.2. Structure at small values of the normalized counting time is reduced for all of the point processes, whereas the fractal variability at large values of the normalized counting time remains essentially intact or, in the case of the HEARTBEAT point process, increases.

substantial agreement with each other, but with characteristics that differ from those of the original realization, thereby demonstrating that the distribution of the interevent intervals plays a role in the manifestation of fractal behavior in this process. That is not to say, however, that this is a fractal point process; the fact that changing the interval distribution changes the fractal characteristics of a point process does not mean that it is a fractal object. We have, in fact, definitively shown in Fig. 5.11 that the synapse data, which are well-described by a fractal-lognormal-noise-driven Poisson process, are characterized by a fractal-rate point process.

The exponentialized data displayed in Figs. 11.10 and 11.11 are, for the most part, devoid of the sharp spectral components and Haar-wavelet-variance oscillations evident in the original data.[10] However, the power-law behavior of the curves remains essentially intact in all cases, demonstrating that the fractal behavior of all seven point processes arises principally from the relative ordering of the intervals and not from the distribution of the interevent intervals themselves. Behavior of this kind is the hallmark of a fractal-rate point process.

[10] The consequences of event-time displacement are similar (see Figs. 11.7 and 11.8). Both are associated with a jittering of the event times, which results in a concomitant loss of phase coherence.

11.5 INTERVAL SHUFFLING

Interval shuffling provides a complementary method for introducing additional randomness into a point process. The shuffling operation randomly reorders the set of interevent intervals $\{\tau_n\}$, thereby destroying any correlations or dependencies that might have existed among them.

Figure 11.12 illustrates how to implement the shuffling operation. The original point process depicted in (a) happens to have events clustered towards the left, corresponding to a rate that effectively decreases with time. The shuffled version in (b) exhibits no such global behavior. Although any possible rearrangement of the original sequence $\{\tau_n\}$ can occur in principle, those with long-term structure, such

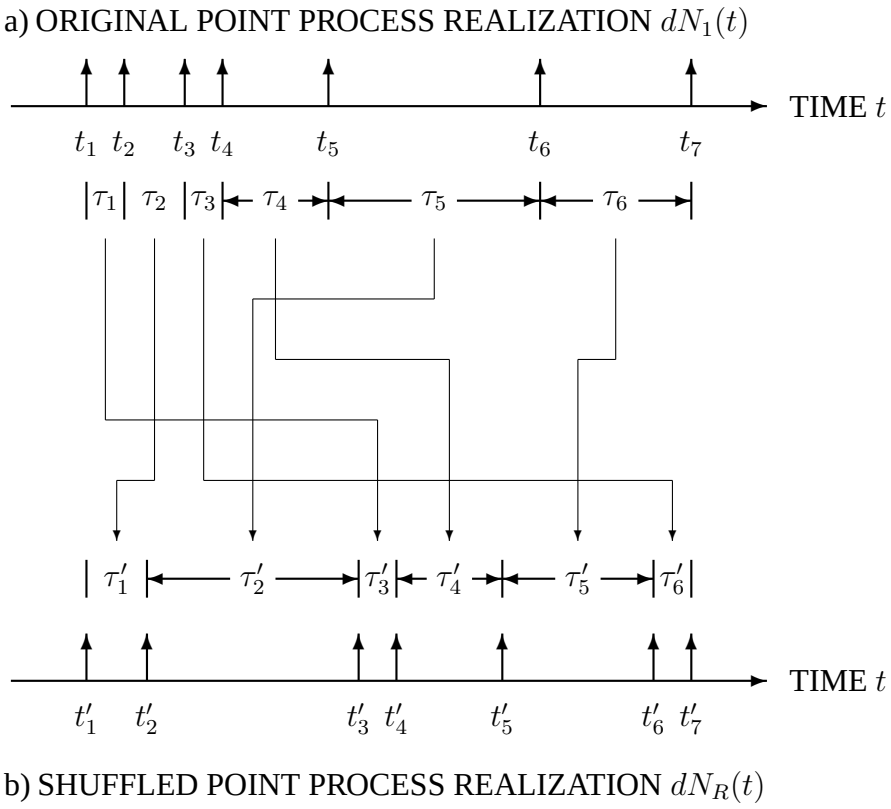

Fig. 11.12 Shuffled point process. (a) The original point process realization has seven event times $\{t_n\}$ and therefore six interevent intervals $\{\tau_n\}$. (b) Randomly reordering the interevent intervals $\{\tau_n\}$ of the original realization yields the interevent intervals $\{\tau'_n\}$ of the shuffled realization. For the particular shuffling illustrated, we have $\tau'_1 = \tau_2$, $\tau'_2 = \tau_5$, $\tau'_3 = \tau_1$, $\tau'_4 = \tau_4$, $\tau'_5 = \tau_6$, and $\tau'_6 = \tau_3$. Assuming the same start time ($t'_1 = t_1$) and employing the relation $\tau'_n = t'_{n+1} - t'_n$ yields the seven event times $\{t'_n\}$ of the shuffled realization.

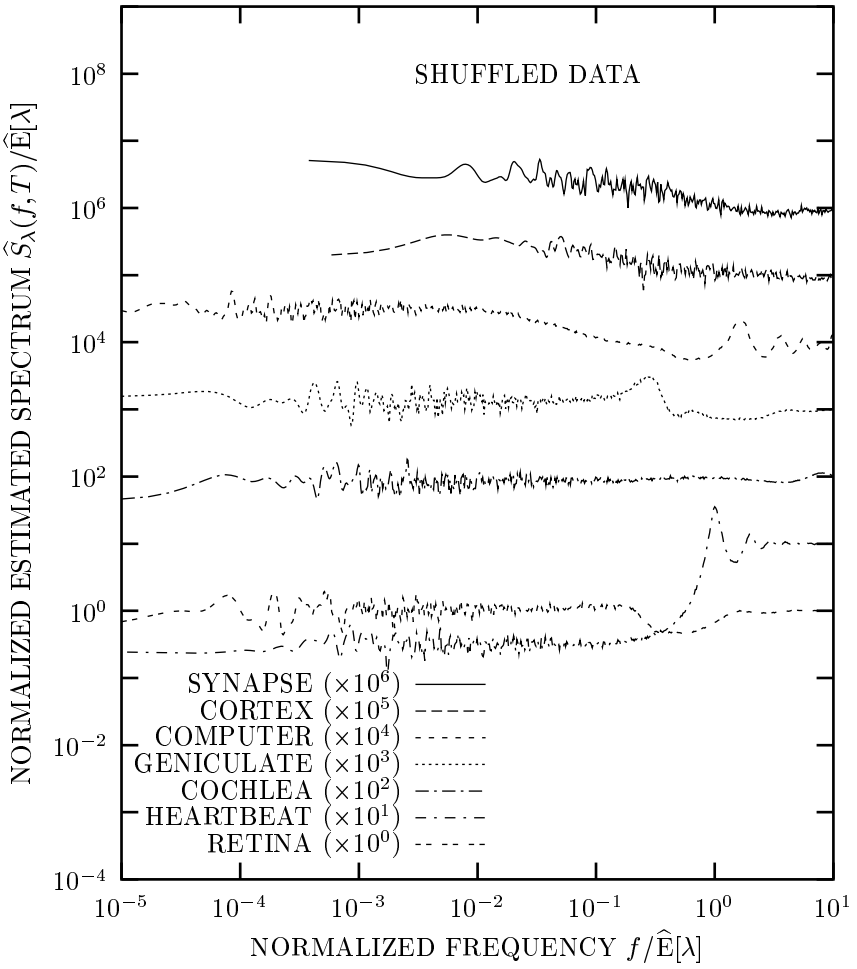

Fig. 11.13 Normalized estimated spectrum after random shuffling, $\widehat{S}_\lambda(f,T)/\widehat{\mathrm{E}}[\lambda]$ vs. normalized frequency $f/\widehat{\mathrm{E}}[\lambda]$, for the six biological point processes and one computer network traffic trace illustrated in Fig. 5.1. The curves are flat for low frequencies, indicating that no vestiges of fractal behavior remain in the shuffled processes.

as a decreasing rate or fractal fluctuations in the sizes of the intervals, prove much less likely. The end result resembles a renewal point process.

Rather than generating new point processes, shuffling typically finds use as a nonparametric method for testing a hypothesis in a point-process realization (Schiff & Chang, 1992; Theiler et al., 1992; Theiler & Prichard, 1996; Schreiber & Schmitz, 1996). A series of independent shufflings of such a realization yields a set of statistically independent reorderings of the same set of interevent intervals $\{\tau_n\}$, and

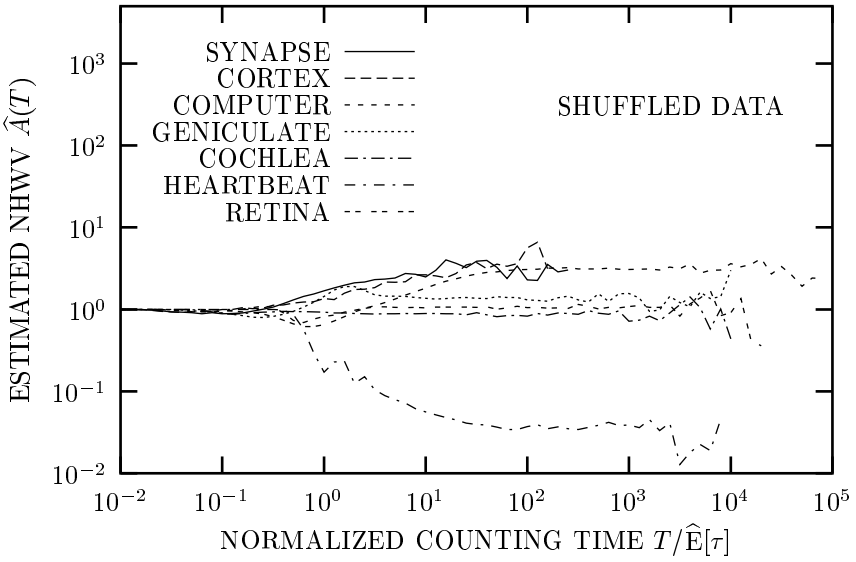

Fig. 11.14 Estimated normalized Haar-wavelet variance (NHWV) following random shuffling, $\widehat{A}(T)$ vs. normalized counting time $T/\widehat{\mathrm{E}}[\tau]$, for the same seven point processes as displayed in Fig. 5.2. The flattening of all of the curves indicates the absence of fractal behavior in all of the shuffled processes.

reveal the likelihood that a particular feature of the realization occurred by chance. For example, the rate spectrum $S_\lambda(f,T)$ can be used to test for nonrenewal behavior. If a number of independent shufflings yield estimates of the spectrum that are in substantial agreement with each other, but differ from that of the original unshuffled process, then the original point process likely has dependent interevent intervals and therefore does not derive from a renewal point process.

Like displacement, interval shuffling destroys any structure present in the original point process $dN_1(t)$, but in this case over time scales smaller than the shuffling, replacing it with (locally) renewal behavior at those scales. In contrast to interval transformation, the relative ordering of the interevent intervals is destroyed but the overall interval distribution is maintained. Indeed, the two operations are complementary, each preserving what the other destroys. The shuffling operation tests the hypothesis that behavior in a particular measure derives from the ordering of the interevent intervals.

In Figs. 11.13 and 11.14 we illustrate the effects of random shuffling on the spectra and normalized Haar-wavelet variances of the canonical set of point processes shown in Figs. 5.1 and 5.2. (We do not display shuffled interevent-interval histograms since they are identical to the original histograms.) The results are dramatic. The shuffling eliminates all vestiges of fractal behavior in all of the processes; it results in a flattening of all curves for both measures. The surrogates considered previously,

random deletion (Figs. 11.3 and 11.4), event-time displacement (Figs. 11.7 and 11.8), and exponentialization (Figs. 11.10 and 11.11), behave quite differently.

However, shuffling an interval-exponentialized realization, or exponentializing a shuffled realization, essentially yields a homogeneous Poisson process (Prob. 11.1).

11.5.1 Block shuffling

Finally, we mention two variations on the theme of shuffling. The first variation, known as **block shuffling**, consists of shuffling intervals within sections of a realization, while keeping intervals from different sections from commingling. For example, one can divide a realization into blocks of k interevent intervals and shuffle the intervals within each block separately. Or, one can divide the realization into contiguous, nonoverlapping periods of duration T and separately shuffle the intervals that begin in each period. These block-shuffling methods preserve fractal and other long-term characteristics over time scales larger than the average block time, while destroying all dependencies over shorter time scales.

11.5.2 Bootstrap method

The second variation selects intervals with replacement, rather than rearranging the intervals; in this case, some of the interevent intervals of the original realization may not appear in the shuffled version, while others can have multiple copies. This approach, called the **bootstrap method**, enjoys some mathematical advantages since it generates renewal processes based on an interevent-interval distribution estimated from the intervals at hand (Efron, 1982; Efron & Tibshirani, 1993). Nevertheless, shuffling without replacement proves superior in some cases, since the set of intervals remains identical. In particular, the mean rate, the total duration of the realization, and all first-order statistics of the interevent intervals do not change.

11.5.3 Identification of fractal-based point processes

With the collection of surrogate-data techniques in hand, we revisit the issue of fractal-based point-process identification. Associating a model with an observed point process is often useful for elucidating mechanisms that underlie the data. We took a first step in this direction in Sec. 5.5.4 (see also Probs. 5.2, 5.3, 5.4, and 5.5) where we showed the possibility of discriminating between fractal and fractal-rate point processes.

What information about the nature of the seven canonical point processes portrayed in Figs. 5.1 and 5.2 might be provided to us by the surrogate-data curves exhibited in Secs. 11.3–11.5?

Fractal behavior manifests itself at low frequencies and large normalized counting times. The displaced surrogates shown in Figs. 11.7 and 11.8 reveal that the fractal behavior does not arise from the details of the local occurrence times for any of the point processes. The exponentialized surrogates presented in Figs. 11.10 and 11.11

inform us further that the fractal behavior is not a result of the particular form of the interevent-interval distribution in any of the point processes.

And, finally, the shuffled surrogates displayed in Figs. 11.13 and 11.14 assure us that, for all of the point processes, the fractal behavior is associated with the ordering of the intervals. The large counting-time asymptotes of $\widehat{A}(T)$ in Fig. 11.14 reveal the clustering characteristics inherent in the interevent-interval distribution, as understood from Eq. (4.18).

We conclude that all seven data sets represent fractal-rate point processes, and not fractal point processes. This conclusion accords with that reached by examining the generalized dimensions D_q of these point processes (see Prob. 5.5). We revisit the issue of fractal-based point-process identification in Secs. 12.1 and 13.6.

11.6 SUPERPOSITION

The superposition $N_R(t)$ of a set of M counting processes, $N_1(t) \ldots N_M(t)$, is formed from their addition. In terms of the point-process formalism, $dN_R(t)$ includes every event in all of the component point processes $dN_k(t)$, as illustrated in Fig. 11.15.

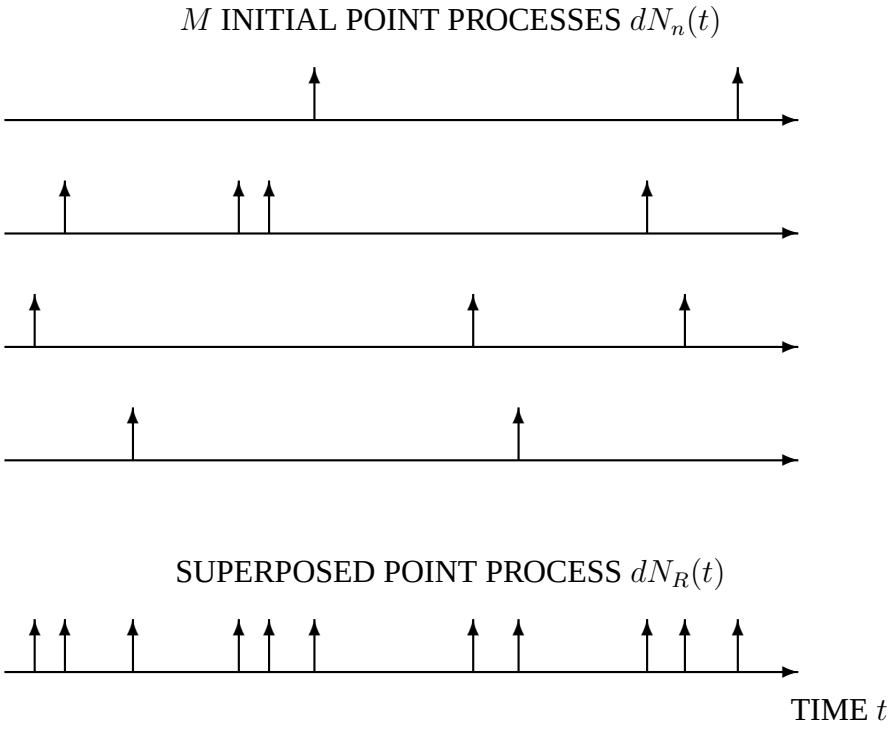

Fig. 11.15 The superposition of M point processes $dN_n(t)$ leads to a process comprising all of the events of the constituent processes. The rate of the superposed process equals the sum of the rates of the constituent point processes, and thus exceeds each of the individual rates.

We therefore have

$$\begin{aligned} N_R(t) &= \sum_{k=1}^{M} N_k(t) \\ dN_R(t) &= \sum_{k=1}^{M} dN_k(t). \end{aligned} \tag{11.39}$$

Palm[11] (1943) appears to have been the first to examine the superposition of point processes; Çinlar (1972) studied this operation extensively.

In broad terms, the superposition of identical fractal and fractal-rate point processes yields results that resemble those for event deletion, in that the characteristic times of the process change but the fractal exponent remains the same.

The most fruitful mathematical approach for examining this problem appears to use the coincidence rate of the resulting point process $dN_R(t)$. We begin with the definition of this quantity for $dN_R(t)$, as presented in Eqs. (3.48) and (3.49):

$$\begin{aligned} G_R(t) &\equiv \lim_{\epsilon \to 0} \epsilon^{-2} \Pr\{N_R(s+\epsilon) - N_R(s) > 0 \\ &\qquad \text{and } N_R(s+t+\epsilon) - N_R(s+t) > 0\} \\ &= \mathrm{E}\left[\frac{dN_R(s)}{ds}\,\frac{dN_R(s+t)}{ds}\right] \\ &= \mathrm{E}\left[\sum_{m=1}^{M} \frac{dN_m(s)}{ds} \sum_{n=1}^{M} \frac{dN_n(s+t)}{ds}\right] \\ &= \sum_{m=1}^{M}\sum_{n=1}^{M} \mathrm{E}\left[\frac{dN_m(s)}{ds}\,\frac{dN_n(s+t)}{ds}\right] \\ &= \sum_{m=1}^{M} \mathrm{E}\left[\frac{dN_m(s)}{ds}\,\frac{dN_m(s+t)}{ds}\right] \\ &\qquad + \sum_{m=1}^{M}\sum_{n\neq m} \mathrm{E}\left[\frac{dN_m(s)}{ds}\,\frac{dN_n(s+t)}{ds}\right] \\ &= \sum_{m=1}^{M} \mathrm{E}\left[\frac{dN_m(s)}{ds}\,\frac{dN_m(s+t)}{ds}\right] \\ &\qquad + \sum_{m=1}^{M}\sum_{n\neq m} \mathrm{E}\left[\frac{dN_m(s)}{ds}\right] \mathrm{E}\left[\frac{dN_n(s+t)}{ds}\right] \\ &= \sum_{m=1}^{M} G_m(t) + \sum_{m=1}^{M}\sum_{n\neq m} \mathrm{E}[\mu_m]\,\mathrm{E}[\mu_n] \end{aligned} \tag{11.40}$$

[11] A photograph of Palm appears at the beginning of Chapter 13.

$$
\begin{aligned}
&= \sum_{m=1}^{M} \Big\{ G_m(t) - \mathrm{E}^2[\mu_m] \Big\} + \sum_{m=1}^{M} \sum_{n=1}^{M} \mathrm{E}[\mu_m]\, \mathrm{E}[\mu_n] \\
&= \sum_{m=1}^{M} \Big\{ G_m(t) - \mathrm{E}^2[\mu_m] \Big\} + \mathrm{E}^2[\mu_R], \qquad (11.41)
\end{aligned}
$$

where the independence of the M point processes yields Eq. (11.40) and the last step leading to Eq. (11.41) results from the fact that the sum of the rates is equal to the rate of the sum. The second-order properties of the superposed process $dN_R(t)$ are simply given by the sum of those for the constituent processes. Equation (11.41) simplifies for constituent processes with identical statistics, whereupon

$$G_R(t) = MG_1(t) + \mathrm{E}^2[\mu_R]\,(1 - 1/M). \qquad (11.42)$$

Turning now to the frequency domain, and considering point processes that have identical fractal characteristics, we have

$$
\begin{aligned}
S_R(f) &= MS_1(f) + \mathrm{E}^2[\mu_R]\,(1 - 1/M)\,\delta(f) \\
&= M\big\{ \mathrm{E}^2[\mu_1]\,\delta(f) + \mathrm{E}[\mu_1]\left[1 + (f/f_{S1})^{-\alpha}\right] \big\} \\
&\quad + \mathrm{E}^2[\mu_R]\,(1 - 1/M)\,\delta(f) \\
&= \mathrm{E}^2[\mu_R]\,\delta(f) + \mathrm{E}[\mu_R]\left[1 + (f/f_{S1})^{-\alpha}\right], \qquad (11.43)
\end{aligned}
$$

which differs from $S_1(f)$ only in the mean rate. In particular, fractal onset times and frequencies remain unchanged under point-process superposition, as do fractal exponents.

11.6.1 Superposition of doubly stochastic Poisson point processes

In general, superposition changes the nature of a point process (Palm, 1943). Doubly stochastic Poisson processes provide the sole exception; superposing M identical processes in this class yields a new point process that differs from the originals only in that its rate is a factor of M larger. Indeed, for a set of arbitrary point processes $dN_1(t), dN_2(t), \ldots$, as M increases $dN_R(t)$ tends towards a doubly stochastic point process with a rate process identical to that of the constituent processes (Çinlar, 1972; Cox & Isham, 1980).

The homogeneous Poisson point process forms a special case. The superposition of this process $dN_1(t)$, and a fractal-rate doubly stochastic Poisson processes $dN_2(t)$, becomes a different doubly stochastic Poisson processes $dN_R(t)$, which is closely related to $dN_2(t)$. The resulting process $dN_R(t)$ shares fractal exponents with $dN_2(t)$, and differs only in its fractal onset times and frequencies.

Setting terms in the spectra of $dN_2(t)$ and $dN_R(t)$ equal, Eq. (5.44a) yields

$$
\begin{aligned}
(\mathrm{E}[\mu_1] + \mathrm{E}[\mu_2])\,(f/f_{SR})^{-\alpha} &= \mathrm{E}[\mu_2]\,(f/f_{S2})^{-\alpha} \\
(f_{SR}/f_{S2})^{\alpha} &= \frac{\mathrm{E}[\mu_2]}{\mathrm{E}[\mu_1] + \mathrm{E}[\mu_2]}. \qquad (11.44)
\end{aligned}
$$

Straightforward application of Eq. (5.45) then yields

$$(T_{F2}/T_{FR})^\alpha = (T_{A2}/T_{AR})^\alpha = (T_{R2}/T_{RR})^\alpha = \frac{\mathrm{E}[\mu_2]}{\mathrm{E}[\mu_1] + \mathrm{E}[\mu_2]}\,, \qquad (11.45)$$

and $t_{GR} = t_{G2}$.

More generally, consider the superposition of a number of independent, identical fractal-based point processes with aggregate rate $\mathrm{E}[\mu_2]$, and a number of independent point processes lacking long-term correlations with aggregate rate $\mathrm{E}[\mu_1]$. The former converge to a fractal-based doubly stochastic Poisson point process whereas the latter converge to a homogeneous Poisson point process. Together, the superposition yields results similar to those of Eqs. (11.44) and (11.45).

11.6.2 Superposition of renewal point processes

For the particular case of superposed renewal point processes, the resulting process $dN_R(t)$ does not belong to the class of renewal point processes, but we may still solve for the interevent interval density function (Cox & Isham, 1980; Ryu & Lowen, 1996).

Consider M independent and identical renewal point processes, with a mean interevent time $\mathrm{E}[\tau_1]$, interevent-interval probability density function $p_{\tau 1}(t)$, and associated survivor function $\mathsf{S}_{\tau 1}(t) \equiv \Pr\{\tau_1 > t\} = \int_t^\infty p_{\tau 1}(u)\,du$. The forward recurrence time $\vartheta_1(t)$, defined in Eq. (3.10), is the time that remains to the next event from an arbitrary starting time. This quantity has a survivor function $\mathsf{S}_{\vartheta 1}(t)$ given by Eq. (3.11). In terms of $p_{\tau 1}(t)$, we therefore have

$$\begin{aligned}
\mathsf{S}_{\vartheta 1}(t) &= \mathrm{E}[\mu_1] \int_t^\infty \mathsf{S}_{\tau 1}(u)\,du \\
&= \mathrm{E}[\mu_1] \int_{u=t}^\infty \int_{v=u}^\infty p_{\tau 1}(v)\,dv\,du \\
&= \mathrm{E}[\mu_1] \int_{v=t}^\infty \int_{u=t}^v p_{\tau 1}(v)\,dv\,du \\
&= \mathrm{E}[\mu_1] \int_t^\infty (v-t) p_{\tau 1}(v)\,dv, \qquad (11.46)
\end{aligned}$$

which denotes the probability of zero arrivals in the renewal process during a period of duration t that starts at a random time independent of the process.

For M independent identical renewal point processes, the probability of zero events occurring in any of the M processes in a time t is simply the product of the probabilities from the individual processes. Therefore, the forward recurrence-time survivor function for the superposed process, $\mathsf{S}_{\vartheta R}(t)$, becomes

$$\begin{aligned}
&\mathrm{E}[\mu_R] \int_t^\infty (v-t)\, p_{\tau R}(v)\,dv \\
&\quad = \mathsf{S}_{\vartheta R}(t)
\end{aligned}$$

$$
\begin{aligned}
&= \left[\mathsf{S}_{\vartheta 1}(t)\right]^M \\
&= \mathrm{E}^M[\mu_1]\left[\int_t^\infty (v-t)\,p_{\tau 1}(v)\,dv\right]^M . \qquad (11.47)
\end{aligned}
$$

After two differentiations and some algebra (Ryu & Lowen, 1996), we obtain the interevent-interval probability density function for the superposed process:

$$
\begin{aligned}
p_{\tau R}(t) &= \mathrm{E}[\tau_1]^{-(M-1)}\left[\int_t^\infty (v-t)\,p_{\tau 1}(v)\,dv\right]^{M-2} \\
&\times \left\{(M-1)\left[\int_t^\infty p_{\tau 1}(v)\,dv\right]^2\right. \\
&\qquad \left. + p_{\tau 1}(t)\int_t^\infty (v-t)\,p_{\tau 1}(v)\,dv\right\}. \qquad (11.48)
\end{aligned}
$$

Two limiting conditions emerge. First, for small interevent times, such that $P_{\tau 1}(t) \ll 1/M$, the probability of two events occurring in the same constituent process approaches zero. In this case we have

$$
\begin{aligned}
\mathsf{S}_{\vartheta R}(t) &= \left[\mathsf{S}_{\vartheta 1}(t)\right]^M \\
&\approx \left(1-\mathrm{E}[\mu_1]\,t\right)^M \\
&\approx 1 - M\,\mathrm{E}[\mu_1]\,t = 1-\mathrm{E}[\mu_R]\,t \\
&\approx \exp\left(-\mathrm{E}[\mu_R]\,t\right). \qquad (11.49)
\end{aligned}
$$

This result is the same as that obtained for a homogeneous Poisson process with the same rate; in fact, $dN_R(t)$ resembles the homogeneous Poisson process over these short time scales. Second, for long times, such that $\mathsf{S}_{\tau 1}(t) \ll 1$, we similarly find that $\mathsf{S}_{\tau R}(t) \ll 1$. In particular, $P_{\tau 1}(t) = 1$ implies that $P_{\tau R}(t) = 1$.

We now specialize to the particular case of a fractal renewal point process with abrupt cutoffs, in which case the interevent-interval probability density function assumes the form of Eq. (7.1); we focus on the limit $A \ll t \ll B$:

$$
p_{\tau 1}(t) = \frac{\gamma}{A^{-\gamma}-B^{-\gamma}} \times \begin{cases} t^{-(\gamma+1)} & \text{for } A < t < B \\ 0 & \text{otherwise.} \end{cases} \qquad (11.50)
$$

For $0 < \gamma < 1$, to first order the forward recurrence-time survivor function follows the form

$$
\mathsf{S}_{\vartheta 1}(t) \approx 1 - \gamma^{-1}(t/B)^{1-\gamma}, \qquad (11.51)
$$

so that

$$
\mathsf{S}_{\vartheta R}(t) \approx \left[1-\gamma^{-1}(t/B)^{1-\gamma}\right]^M \approx 1 - M\gamma^{-1}(t/B)^{1-\gamma}. \qquad (11.52)
$$

Substituting Eq. (11.52) into Eq. (3.12), and taking another derivative, yields the corresponding interevent interval probability density function

$$p_{\tau R}(t) \approx \gamma A^{\gamma} t^{-(\gamma+1)}, \tag{11.53}$$

identical to $p_{\tau 1}(t)$ over that time scale. Taken together, Eqs. (11.52) and (11.53) indicate that for $0 < \gamma < 1$ and $A \ll t \ll B$, the time statistics for the superposed process resemble those of a single fractal renewal process, with the upper cutoff B replaced by the smaller value $M^{1/(\gamma-1)}B$. The superposition process modifies the interval probability density only slightly for moderate values of M. Achieving an approximate Poisson-process form requires on the order of $M = (B/A)^{1-\gamma}$ fractal renewal processes.

The situation changes for larger values of γ. For $\gamma > 1$, the same procedure yields

$$\mathsf{S}_{\vartheta 1}(t) \approx \gamma^{-1}(t/A)^{1-\gamma} \tag{11.54}$$

$$\mathsf{S}_{\vartheta R}(t) \approx \gamma^{-M}(t/A)^{M(1-\gamma)} \tag{11.55}$$

$$p_{\tau R}(t) \approx c\,\gamma^{1-M} A^{c} t^{-(c+1)}, \tag{11.56}$$

where we define $c \equiv 1 + M(\gamma - 1)$ and note that $c > 1$. Thus, the survivor function of the superposition decays progressively more quickly as we add more fractal renewal processes, approaching the exponential limit of the Poisson process far more quickly than in the domain $0 < \gamma < 1$. For $\gamma = 1$, intermediate results obtain; the superposition approaches Poisson form slowly as M increases, but not as slowly as when $\gamma < 1$.

Problems

11.1 *Shuffled and exponentialized point processes* Show that shuffling a fractal-based point process and transforming its intervals to an exponentially distributed form, in either order, must result in a homogeneous Poisson process.

11.2 *Superposed fractal-based point processes* Consider two fractal-based point processes, $dN_1(t)$ and $dN_2(t)$, whose superposition yields another process $dN_R(t)$.

11.2.1. Under what conditions does $dN_R(t)$ precisely follow the power-law form of Eq. (5.44)?

11.2.2. Under those conditions, find α_R, $\mathrm{E}[\mu_R]$, and f_{SR} in terms of the related parameters for $dN_1(t)$ and $dN_2(t)$.

11.2.3. Under what set of more-relaxed conditions does $dN_R(t)$ closely approximate a fractal form?

11.3 *Interval transformation and shuffling as surrogates* Both interevent-interval transformation (Sec. 11.4) and shuffling (Sec. 11.5) modify fractal-based point processes in ways that yield insights into the processes under study. Suppose that we evaluate the spectrum of a point process before and after shuffling, and compare the results. For simplicity, we consider three classes of results: (1) shuffling leaves the spectrum essentially unchanged; (2) shuffling effectively eliminates the fractal character of the process; and (3) shuffling decreases the fractal onset frequency, thereby

leading to a process with decreased, but still present, fractal content. We also examine the same three classes for the interevent-interval transformation. Consider each of the nine possible pairs of classes. Determine which pairs cannot occur and, for the others, describe processes that could yield those results.

11.4 *Fractal content of superposed point processes* We can quantify the fractal content in a fractal-based point process, discussed in Prob. 11.3, with a dimensionless quantity such as $c_f \equiv f_S/\mathrm{E}[\mu]$, which remains constant under time dilation. Consider a fractal-based point process $dN_R(t)$, formed by the superposition of two component fractal-based point processes $dN_1(t)$ and $dN_2(t)$ with the same fractal exponent α. Under what conditions does c_{fR} equal or exceed both c_{f1} and c_{f2}?

11.5 *Statistics of a dilated and deleted point process* We can scale the time axis in a fractal-rate point process $dN_1(t)$ to effectively double its rate, yielding $dN_2(t)$, and we can then delete half of the events in $dN_2(t)$ to yield a new process $dN_R(t)$ closely related to the first. Assume that the deletion process does not selectively affect the low-frequency components of the point process.

11.5.1. How do the mean rate $\mathrm{E}[\mu]$, fractal exponent α, and fractal onset frequency f_S compare for $dN_R(t)$ and $dN_1(t)$?

11.5.2. Suppose that $dN_1(t)$ is (a) a homogeneous Poisson process or (b) an integrate-and-reset process with constant rate; and that we delete events either (1) randomly and independently and retaining half of them or (2) by decimation in which every other event is retained. What type of point-process results in each of the four cases?

11.6 *Homogeneous Poisson process modified by fixed and stochastic dead time* Suppose a homogeneous Poisson process $dN_1(t)$ with rate μ_1 experiences a fixed dead time of duration τ_f, followed by an exponentially distributed stochastic dead time of expected duration τ_r. The resulting process $dN_R(t)$ becomes a dead-time-modified homogeneous Poisson process. Determine the nature of this point process, as well as the mean and variance of the interevent interval, the rate, the interevent-interval probability density, and the associated characteristic function. Finally, for the special case $\tau_r = 0$, find the spectrum.

11.7 *Forward-recurrence-time survivor function for a fractal renewal process* Prove Eqs. (11.51)–(11.56) in greater detail.

11.8 *Modification of a point process by block shuffling and event-time displacement* Consider a doubly stochastic Poisson process $dN_1(t)$ driven by a fractal rate. The spectrum of this process, $S_{N1}(f)$, follows Eq. (5.44a) over a wide range of frequencies.

11.8.1. Now suppose we divide the time axis into contiguous blocks of duration T. Effect a block shuffle of the process by taking all interevent intervals that begin in each block and shuffle them with each other, but not with intervals beginning in other blocks. For $f_S T = 100$, sketch the spectrum $S_{NR}(f)$ of the resulting block-shuffled process $dN_R(t)$.

11.8.2. Instead of block shuffling, we now add to each event time t_k a Gaussian-distributed random number with zero mean and standard deviation equal to $100/f_S$, as illustrated in Eq. (11.38). We then sort the displaced event times back into ascending order and define $dN_R(t)$ in terms of the resulting sorted set of event times. Sketch the spectrum $S_{NR}(f)$ of this displaced process $dN_R(t)$.

11.9 *Properties of a randomly deleted renewal process* Let $dN_1(t)$ denote a renewal point process with interevent-interval probability density $p_\tau(t)$.

11.9.1. Show that independently deleting events in $dN_1(t)$ with a probability r yields another renewal point process $dN_R(t)$.

11.9.2. Find the interevent-interval probability density of $dN_R(t)$.

11.9.3. Using characteristic functions, examine the behavior of $dN_R(t)$ for the specific case where $dN_1(t)$ has the abrupt power-law probability density exhibited in Eq. (7.1). Focus on the medium-time limit $A \ll t \ll B$. How do results for $0 < \gamma < 1$ and $\gamma \geq 1$ differ?

11.10 *Dead-time-modified and decimated Poisson counting distributions* The counting distribution for the dead-time-modified homogeneous Poisson process proves useful in many contexts, including nuclear, neural, and photon counting (DeLotto et al., 1964; Ricciardi & Esposito, 1966; Müller, 1973; Cantor & Teich, 1975; Libert, 1976; Teich & Cantor, 1978; Müller, 1981; Prucnal & Teich, 1983). The formula is considerably more complex than Eq. (4.7) for the Poisson counting distribution as a result of correlation between the numbers of events in adjacent counting windows, engendered by the occurrence of the dead-time periods that straddle them. The counts $\{Z_k(T)\}$ are therefore not independent.

For the nonparalyzable dead-time counter unblocked at the beginning of the counting interval (see Footnote 6 on p. 236), the exact result is (Ricciardi & Esposito, 1966; Müller, 1974; Prucnal & Teich, 1983):

$$p_Z\big(n;T\big) = \Pr\big\{N(t+s) - N(s) = n\big\}$$

$$= \begin{cases} \displaystyle\sum_{m=0}^{n} \frac{\big[\mu_1 T(1-n\tau_e/T)\big]^m}{m!}\, \exp\big[-\mu_1 T(1-n\tau_e/T)\big] \\ \qquad \displaystyle - \sum_{m=0}^{n-1} \frac{\big[\mu_1 T(1-(n-1)\tau_e/T)\big]^m}{m!}\, \exp\big[-\mu_1 T(1-(n-1)\tau_e/T)\big] \\ \qquad\qquad\qquad\qquad\qquad\qquad \text{for } \ 0 \leq n < T/\tau_e, \\ \\ \displaystyle 1 - \sum_{m=0}^{n-1} \frac{\big[\mu_1 T(1-(n-1)\tau_e/T)\big]^m}{m!}\, \exp\big[-\mu_1 T(1-(n-1)\tau_e/T)\big] \\ \qquad\qquad\qquad\qquad\qquad\qquad \text{for } \ T/\tau_e \leq n < T/\tau_e + 1, \\ \\ 0 \qquad\qquad\qquad\qquad\qquad\qquad\qquad\qquad \text{for } \ n \geq T/\tau_e + 1, \end{cases} \tag{11.57}$$

where μ_1 is the driving rate of the process before the imposition of the fixed dead-time period τ_e. The rate after dead-time modification is $\mathrm{E}[\mu_R] = \mu_1/(1+\mu_1\tau_e)$ [see Eq. (11.22)].

Results for various kinds of dead-time counters are available (Müller, 1973, 1974; Libert, 1976); exact formulas for *equilibrium* (stationary) and *blocked* (ordinary) counting distributions resemble Eq. (11.57) for the *unblocked* (shifted or free) result provided above, but they are more complex. In the usual situation when the mean count greatly exceeds unity, the differences among the blocked, unblocked, and equilibrium counting results are, in fact, insubstantial and all three of these processes may essentially be viewed as stationary equivalents of each other (Libert, 1976).

Decimation of a homogeneous Poisson process with decimation parameter m yields the integer-order gamma renewal process of index m (see Sec. 11.2.2 and Prob. 4.7). In this case, the counting distribution takes the form of a finite sum of Poisson distributions, provided that the process is turned on at $t = 0$ (Parzen, 1962; Cox, 1962; Cox & Isham, 1980; Teich et al., 1984, Eq. (A26)):

$$p_Z(n;T) = \sum_{l=\mathsf{m}n}^{\mathsf{m}n+\mathsf{m}-1} \frac{(\mu_1 T)^l \, \exp(-\mu_1 T)}{l!}, \qquad n \geq 0; \tag{11.58}$$

the rate of the initial Poisson process is μ_1 and the decimated rate $\mathrm{E}[\mu_R] \approx \mu_1/\mathsf{m}$.[12] This formula comes about because the integer-order gamma process arises from the homogeneous Poisson process by permitting every mth event to survive, while deleting intermediate events, as illustrated in Fig. 11.1b).

11.10.1. Simulate (or plot) the counting distribution for the nonparalyzable dead-time-modified Poisson process for $\mu_1 T = 15$ and $\mu_1 \tau_e = 0, 0.2, 0.5,$ and 1.0. Confirm that the count mean and count variance agree with $\mathrm{E}[\mu_R]\, T = \mu_1 T/(1 + \mu_1 \tau_e)$ and $\mathrm{Var}[n] \approx \mu_1 T/(1 + \mu_1 \tau_e)^3$, respectively.

11.10.2. Now simulate (or plot) the counting distribution using values of μ_1 that are adjusted such that the count mean *after* dead-time modification is $\mathrm{E}[\mu_R]\, T = 15$ for all values of $\mu_1 \tau_e$. Compare the distributions.

11.10.3. Explain qualitatively how the count mean and variance would differ if the dead-time operation were imposed on a Poisson process with a slowly varying fractal rate instead of on a homogeneous Poisson process.

11.10.4. Simulate the counting distribution for a decimated Poisson process with $\mu_1 T = 15$ and $\mathsf{m} = 1$, 0.5, 1.5, and 2.0. Confirm that the same curve emerges from Eq. (11.58) for $\mathsf{m} = 1$ and 2 (this equation is suitable only for integer values of m). Confirm that the count mean and count variance follow $\mathrm{E}[\mu_R]\, T \approx \mu_1 T/\mathsf{m}$ and $\mathrm{Var}[n] \approx \mu_1 T/\mathsf{m}^2$, respectively.

11.10.5. Finally, simulate the decimated-Poisson process using values of μ_1 that are adjusted such that the count mean *after* decimation is $\mathrm{E}[\mu_R]\, T = 15$ for all values of m. Compare the distributions.

11.11 *Amplification of fractal behavior via exponentialization* The fractal behavior inherent in a 20-hour sequence of heartbeats recorded from a normal human

[12] This approximation asymptotically achieves equality as time increases for this renewal process, which begins with an event. For a starting time selected randomly with respect to the process, the equality holds for all times $t > 0$.

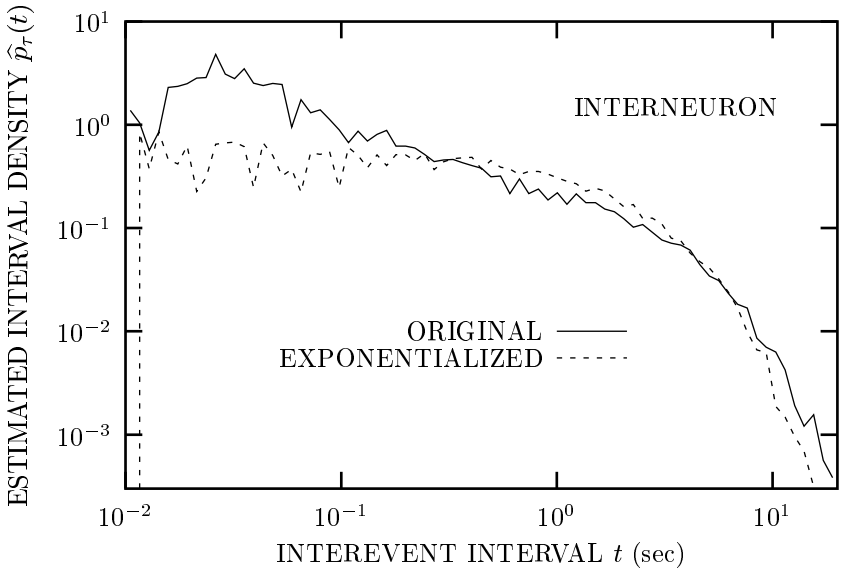

Fig. 11.16 Estimated interevent-interval density, $\widehat{p}_\tau(t)$ vs. interevent interval t, for an action-potential sequence recorded from the descending contralateral movement detector, a visual-system INTERNEURON in the locust (Turcott et al., 1995, Fig. 2, pp. 261–262, cell ADA062) (solid curve). The dotted curve represents results for an exponentialized version of these data. We show the normalized Haar-wavelet variance for these same data in Fig. 11.17.

subject (HEARTBEAT) (Turcott & Teich, 1996, data set 16273) increases considerably when we exponentialize the original point process. Comparing Figs. 11.10 and 11.11 with Figs. 5.1 and 5.2 illustrates this effect. Explain why this comes about.

11.12 *Action-potential statistics in an insect visual-system interneuron: Revisited* The solid curve in Fig. 11.16 displays the estimated interevent-interval density for a spontaneous sequence of action potentials observed from a locust visual-system interneuron (the descending contralateral movement detector, Turcott et al., 1995). The solid curve in Fig. 11.17 shows the estimated normalized Haar-wavelet variance $\widehat{A}(T)$, plotted as a function of the counting time T, for the same set of data. These curves were first presented in Figs. 7.8 and 7.9, and Figs. B.4 and B.5, in connection with Prob. 7.8, where we demonstrated that a fractal renewal point process fails to describe this spike train in spite of the fact that the estimated interevent-interval density follows a decaying power-law form.

11.12.1. The dotted curve shown in Fig. 11.16 represents the exponentialized interevent-interval surrogate data discussed in Sec. 11.4.2. The shuffled surrogate discussed in Sec. 11.5 is identical to the original data since the interevent-interval density, by construction, ignores interval ordering. What conclusions can we draw from these curves with respect to the nature of the underlying point process?

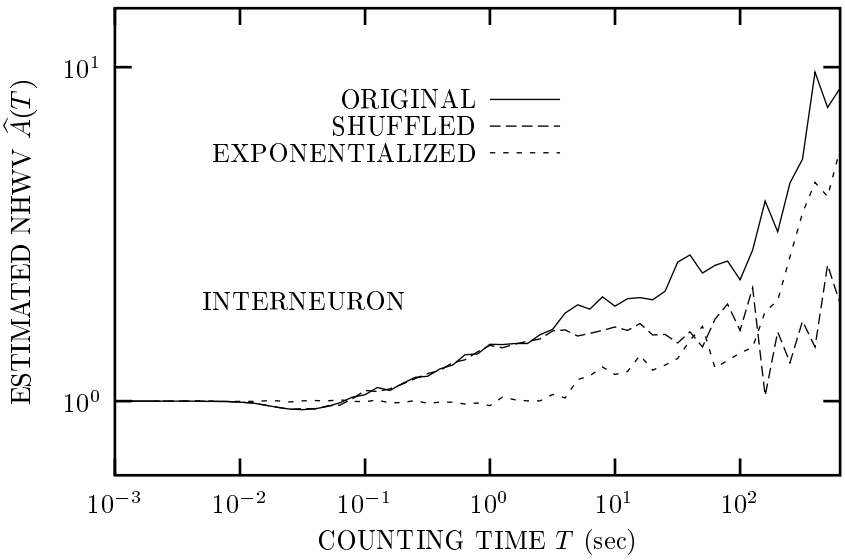

Fig. 11.17 Estimated normalized Haar-wavelet variance $\widehat{A}(T)$ vs. counting time T (sec), for an action-potential sequence recorded from the descending contralateral movement detector, a visual-system INTERNEURON in the locust (Turcott et al., 1995, Fig. 2, pp. 261–262, cell ADA062) (solid curve). Dashed and dotted curves represent results for the shuffled and exponentialized versions of these data, respectively. Unlike the display in Fig. 5.2, the abscissa reports the counting time in unnormalized form. The interevent-interval density appears in Fig. 11.16.

11.12.2. The dashed and dotted curves shown in Fig. 11.17 represent, respectively, the shuffled and exponentialized normalized Haar-wavelet variance surrogate data. What conclusions about the underlying point process can we draw from the behavior of these curves?

11.12.3. Verify that the sum of the shuffled and exponentialized *excess* normalized Haar-wavelet variances, $\widehat{A}(T) - 1$, closely approximates the *excess* normalized Haar-wavelet variance of the original data. What does this signify about the ability of these two surrogates to achieve their intended goals?

11.12.4. Based on all of this information, speculate on the form of a suitable point-process model for characterizing the spike train from the descending contralateral movement detector in the locust.

11.12.5. Figure 11.18 displays generalized-dimension scaling functions for the interneuron data for $q = -1$, 0, $\frac{1}{2}$, 1, and 2. Do these curves support your speculation with respect to a suitable model for the point process, as considered in Prob. 11.12.4?

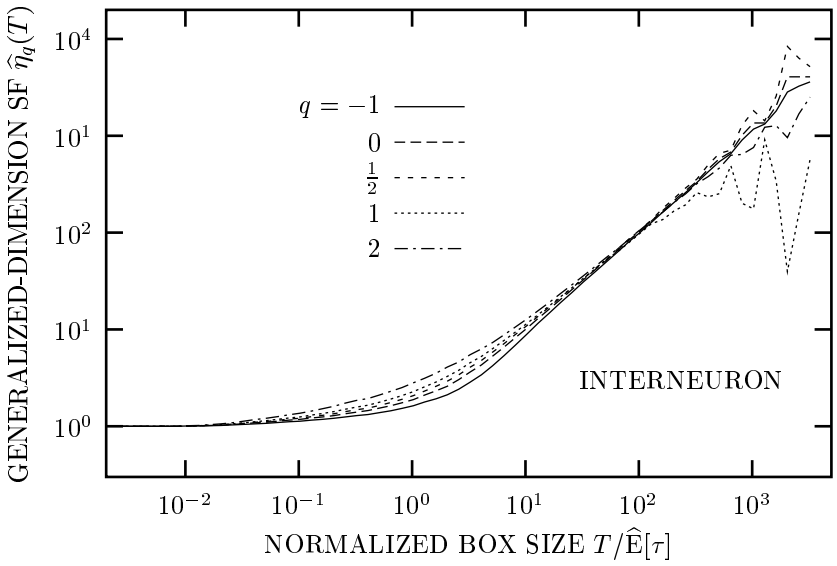

Fig. 11.18 Generalized-dimension scaling functions (SF) $\widehat{\eta}_q(T)$ for various values of q, based on Eq. (3.73), for an action-potential sequence recorded from the descending contralateral movement detector, a visual-system INTERNEURON in the locust (Turcott et al., 1995, cell ADA062). The curves resemble each other, and also those for the nonfractal homogeneous Poisson process (see Fig. B.3). The interevent-interval density and the normalized Haar-wavelet variance for these same data, along with their surrogates, are displayed in Figs. 11.16 and 11.17, respectively. A fractal-rate point process describes these data. Analogous curves for neurotransmitter exocytosis at a SYNAPSE appear in Fig. 5.11.